AD-A074 371 SYSTEMS SCIENCE AND SOFTWARE LA JOLLA CA F/G 18/3
HYDROGEN, OXYGEN, WATER STEAM GENERATOR.(U)
OCT 78 P LAGUS DNA001-77-C-0188
UNCLASSIFIED SSS-R-79-3813 DNA-4733F NL

1 OF 2
AD A074371

(12) LEVEL III

DNA 4733F

HYDROGEN, OXYGEN, WATER STEAM GENERATOR

Systems, Science and Software
P.O. Box 1620
La Jolla, California 92038

15 October 1978

Final Report for Period 18 March 1977—15 October 1978

CONTRACT No. DNA 001-77-C-0188

APPROVED FOR PUBLIC RELEASE;
DISTRIBUTION UNLIMITED.

THIS WORK SPONSORED BY THE DEFENSE NUCLEAR AGENCY
UNDER RDT&E RMSS CODE B345077462 J24AAXYX98351 H2590D.

Prepared for
Director
DEFENSE NUCLEAR AGENCY
Washington, D. C. 20305

Destroy this report when it is no longer needed. Do not return to sender.

PLEASE NOTIFY THE DEFENSE NUCLEAR AGENCY, ATTN: STTI, WASHINGTON, D.C. 20305, IF YOUR ADDRESS IS INCORRECT, IF YOU WISH TO BE DELETED FROM THE DISTRIBUTION LIST, OR IF THE ADDRESSEE IS NO LONGER EMPLOYED BY YOUR ORGANIZATION.

UNCLASSIFIED

SECURITY CLASSIFICATION OF THIS PAGE *(When Data Entered)*

REPORT DOCUMENTATION PAGE

READ INSTRUCTIONS BEFORE COMPLETING FORM

1. REPORT NUMBER: DNA 4733F	2. GOVT ACCESSION NO.
3. RECIPIENT'S CATALOG NUMBER	
4. TITLE *(and Subtitle)*: HYDROGEN, OXYGEN, WATER STEAM GENERATOR	5. TYPE OF REPORT & PERIOD COVERED: Final Report for Period 18 Mar 77—15 Oct 78
6. PERFORMING ORG. REPORT NUMBER: SSS-R-79-3813	
7. AUTHOR(s): Peter Lagus	8. CONTRACT OR GRANT NUMBER(s): DNA 001-77-C-0188
9. PERFORMING ORGANIZATION NAME AND ADDRESS: Systems, Science and Software, P.O. Box 1620, La Jolla, California 92038	10. PROGRAM ELEMENT, PROJECT, TASK AREA & WORK UNIT NUMBERS: Subtask J24AAXYX983-51
11. CONTROLLING OFFICE NAME AND ADDRESS: Director, Defense Nuclear Agency, Washington, D.C. 20305	12. REPORT DATE: 15 October 1978
	13. NUMBER OF PAGES: 110
14. MONITORING AGENCY NAME & ADDRESS *(if different from Controlling Office)*	15. SECURITY CLASS *(of this report)*: UNCLASSIFIED
	15a. DECLASSIFICATION/DOWNGRADING SCHEDULE

16. DISTRIBUTION STATEMENT *(of this Report)*

Approved for public release; distribution unlimited.

17. DISTRIBUTION STATEMENT *(of the abstract entered in Block 20, if different from Report)*

18. SUPPLEMENTARY NOTES

This work sponsored by the Defense Nuclear Agency under RDT&E RMSS Code B345077462 J24AAXYX98351 H2590D.

19. KEY WORDS *(Continue on reverse side if necessary and identify by block number)*

Steam Torch
Hydrogen
Oxygen Steam
Steam Hydrofrac
Porous Media Steam Flow

20. ABSTRACT *(Continue on reverse side if necessary and identify by block number)*

A prototype hydrogen, oxygen, water steam generating system has been developed. The system has been used to generate a modest amount of data relating to steam propagation through a packed sand column. A much larger capacity steam generating system based on the work completed appears to be possible.

DD FORM 1 JAN 73 1473 EDITION OF 1 NOV 65 IS OBSOLETE

UNCLASSIFIED

SECURITY CLASSIFICATION OF THIS PAGE *(When Data Entered)*

388 507

TABLE OF CONTENTS

LIST OF ILLUSTRATIONS

LIST OF ILLUSTRATIONS (continued)

LIST OF TABLES

I. INTRODUCTION

For several years hydrofracture has been recognized as a potential failure mechanism which may compromise the desired containment of underground nuclear explosions. Very little quantitative data exists about hydrofracture processes in the tuff of Area 12 (Nevada Test Site) and no data is available from a steam-driven hydrofrac. The latter is particularly unfortunate since steam is likely to be the medium of concern in any forthcoming test. In addition, the physical processes involved in a condensible medium hydrofrac are more complex than those associated with more conventional gas or liquid hydrofracture systems. For instance, condensible hydrofracture involves the coupled interaction of heat transfer, condensation, gas and liquid diffusion, viscous flow, and crack development phenomena. These various processes have been incorporated into a numerical model, KRAK, developed at the Los Alamos Scientific Laboratory.

During the preceding year, developmental work has been funded (under Contract DNA001-77-C-0188) on an experimental effort to provide quantitative information regarding the feasibility of a steam-driven hydrofracture experiment. During the period of performance of this contract, a rudimentary hydrogen-oxygen-water steam generating system was constructed. It was operated within a sandfilled concrete pipe at the Green Farm Test Site.

The primary objective of this work was to undertake prototype development of a steam-generating torch with an eye toward understanding some of the fundamental engineering problems and limitations which might be encountered in any full-scale effort to produce a bore-hole steam-generating probe.

The second objective of this work was to thoroughly understand the safety limitations and implications of using hydrogen to generate steam in a confined area. Emphasis had to be placed on the problems of using both high pressure hydrogen and oxygen in a controllable and safe manner. Particular attention was paid to the safety aspects of high pressure hydrogen and oxygen systems.

An additional objective of this work was to generate a small amount of data concerning the progress of steam driven through a packed sand column with known characteristics. These data permit the comparison of actual experimental data with predictions of the KRAK code in a simple geometry. All told, nineteen "full-up" experiments of the prototype steam-generating system were performed in a sand packed column. Of these, eight experiments produced data which could be used for comparison with predictions of the KRAK code.

In Section 2 we discuss the physical principles underlying the steam torch.

In Section 3 we present details of the equipment design and test performance.

In Section 4 we present the eight data sets which have useful information and were experimentally successful.

In Section 5 we provide a brief discussion of the data with recommendations for further work and recommendations on the feasibility of a bore-hole steam-generating probe.

In addition, four appendicies are provided. In one, a capacitive saturation monitoring gauge is discussed and data are presented from two successful runs; in the second,

permeability flow measurements in a sand packed column are discussed. In the third appendix, we present physical properties of the liner material used in these experiments. The fourth presents an extensive discussion of the safety aspects of hydrogen handling in general.

II. TECHNICAL DISCUSSION

The objective of the previous year's work was to design, fabricate and test a prototype system utilizing hydrogen, oxygen and water for generating copious quantities of steam possessing known thermodynamic conditions. Quantitative data were obtained on the various flow parameters involved in the generation of the steam. In addition, the system was to be controllable to the point where one could alter the thermodynamic state of the steam from experiment to experiment. These considerations led us to consider utilizing a water cooled hydrogen and oxygen flame. Our initial reaction to the idea was negative because of the obvious safety concern associated with it. On the other hand, the fact that the gases are highly reactive is of major assistance in developing an over-all system. The gas ignition and process control have turned out to be relatively straightforward. Figure 1 demonstrates the range of pure steam conditions available in an adiabatic constant reaction system for the reaction:

$$2H_2(g) + O_2(g) + n\ H_2O\ (\ell) \longrightarrow (n+2)\ H_2O\ (g)$$

In this case the hydrogen and oxygen flame is assumed to be cooled by water spray. Note that temperatures on the order of 1000 to 2000 degress kelvin are generated at pressures of the order of 50 to 100 atmospheres with modest additions of liquid water. These calculations were made for an ideal gas equation of state, with dissociation included. Several non-ideal calculations have shown these results to be reliable to about 1% and dissociation is unimportant at temperatures below 2500 degrees kelvin.

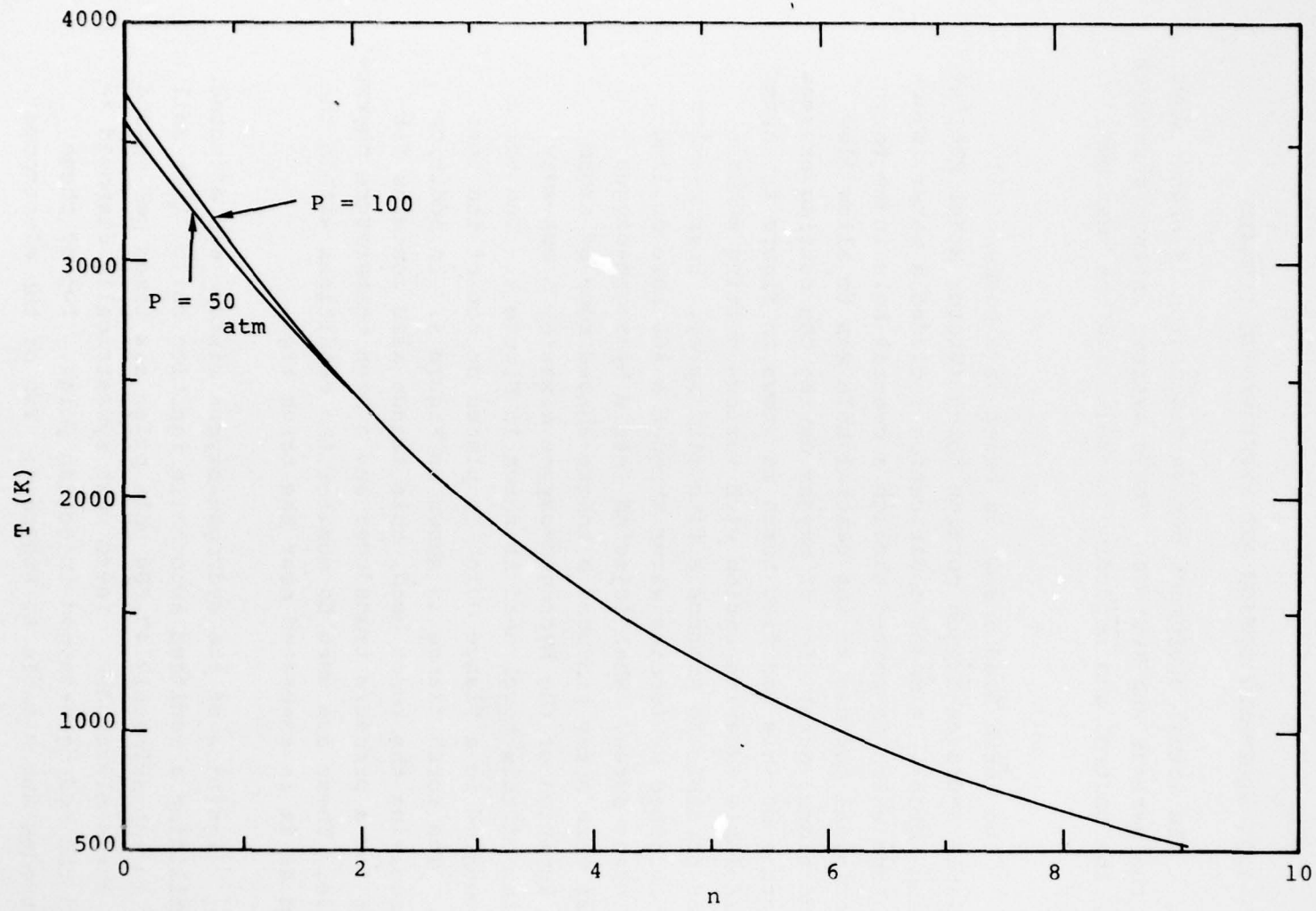

Figure 1. Adiabatic, constant pressure flame temperature ($\Delta H \equiv 0$) for $2H_2 + O_2 + nH_2O(\ell) \rightarrow (n+2)\ H_2O$ ideal gas equation of state assumed.

III. EQUIPMENT DESIGN AND EXPERIMENTAL DETAILS

The actual equipment design discussion is broken down into the various sub-systems. These systems include the torch head, the control and recording console, and the test bed itself.

The torch head design is based on a commercially available hydrogen-oxygen cutting torch (Victor Model MT610AV cutting torch). A major modification included a water injection hose which is ported through a central hole in the torch. The original purpose of the central hole was to allow flow of additional quantities of oxygen during the cutting process. A picture of this modified torch is shown in Figure 2. After considerable experimentation with various porting schemes, it was possible to produce a fine mist spray. Best results were obtained by forcing water through a #60 hole drilled in a brass screw. When injected into a hydrogen-oxygen stream this spray produced a tongue-shaped cone of steam upon ignition of the hydrogen-oxygen mixture. A cut-away drawing of this torch head is shown in Figure 3. The torch was mounted in a flange which is placed on top of the test pipe. The torch flange is shown in Figure 4. In addition to receiving the torch head, this flange also contains fittings for a pressure transducer and a high temperature thermocouple. These are used to monitor the conditions within the steam as it is generated near the torch tip.

Ignition of the hydrogen-oxygen mixture was effected by utilizing a modified automobile ignition coil. This coil sent an approximately 40,000 volt pulse six times per second into three electrodes. These were symmetrically disposed around the hydrogen-oxygen injection point. Two of these electrodes are visible in Figure 4. Two of the electrodes

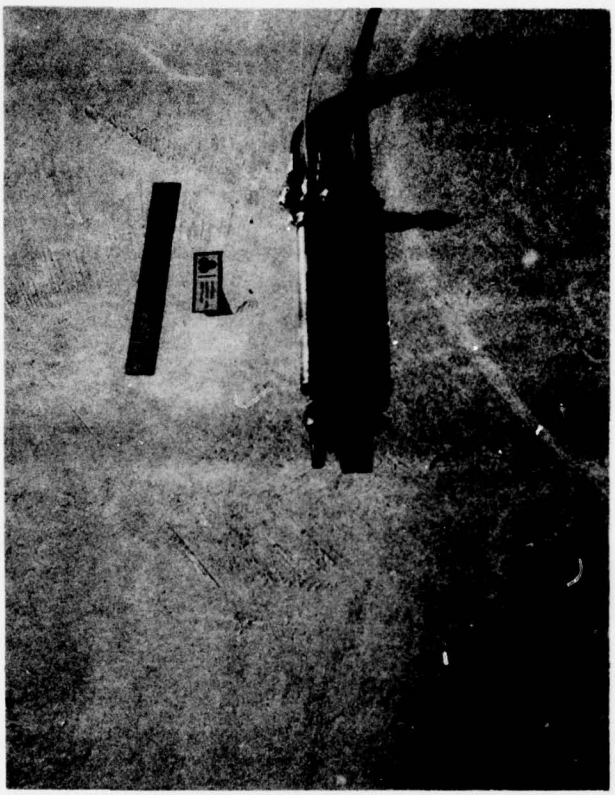

Figure 2. Cutting Torch Head Modified to Accommodate Water Flow

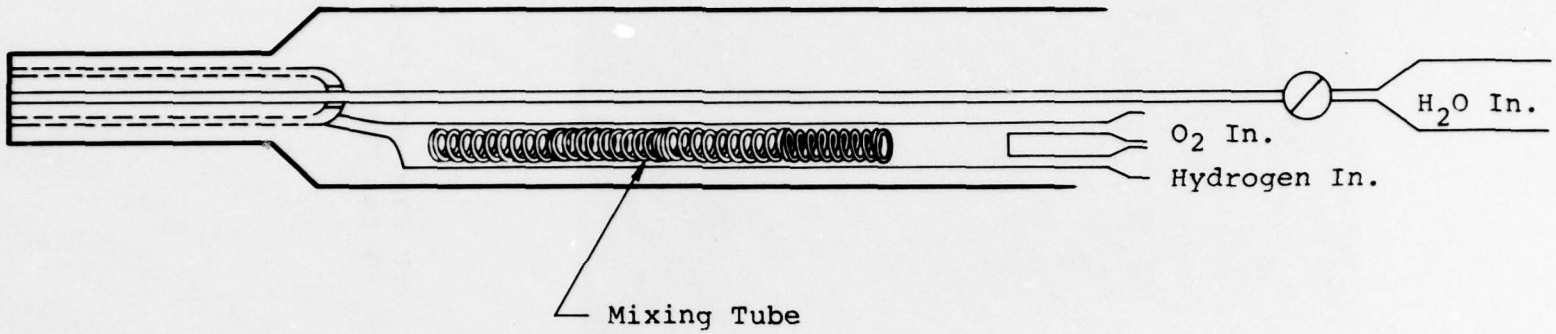

Figure 3. Cutaway drawing of torch head.

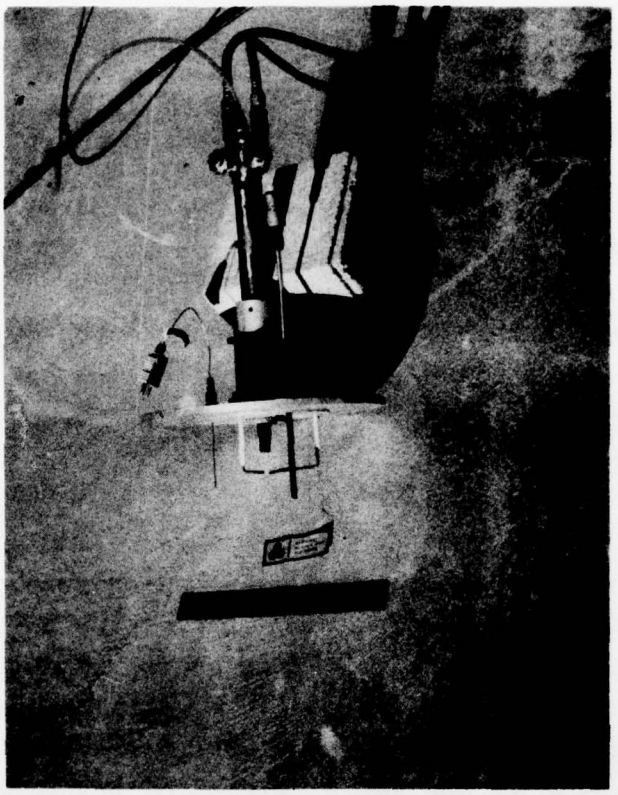

Figure 4. Torch Flange showing torch head in place as well as pressure transducer, thermocouple and sparker electrode.

were positive and arced to a common electrode providing several centimeter-long sparks of 40,000 volts potential. Under the thermodynamic conditions expected to be encountered during these experiments, such sparks are more than sufficient to ignite mixtures of hydrogen and oxygen. A block diagram of the pulsing circuit for the electrodes is shown in Figure 5.

The torch flange is mounted at the top of an approximately 4 meter long transite pipe. A drawing of this is presented in Figure 6. A photograph of the transite pipe mounted adjacent to Bunker B at the Green Farm Test Facility is shown in Figure 7.

The location of the hydrogen and oxygen bottles are also shown in Figure 7. They are outside any area which may be occupied by experimenters during an experiment. Only one person is allowed within the concrete block area when the bottles are connected and opened. The block area has no top. This allows rapid escape and diffusion of any gases which might be released during the connecting of the hydrogen and oxygen lines from the supply bottles to the torch head. Control of the entire experiment as well as monitoring of the thermodynamic conditions near the torch and the passage of steam down the sand filled transite pipe is effected from within the bunker.

The mounting of the torch flange to the test pipe is shown in Figure 8. Positive pressure relief for the system is provided by the springs which begin to release the top flange when the pressure within the chamber reaches 30 psig. This ensures that pressures sufficient to fracture the pipe can not build up within it. The top and bottom flanges are connected by means of three steel rods running the entire length of the transite pipe. By adjusting turnbuckles on

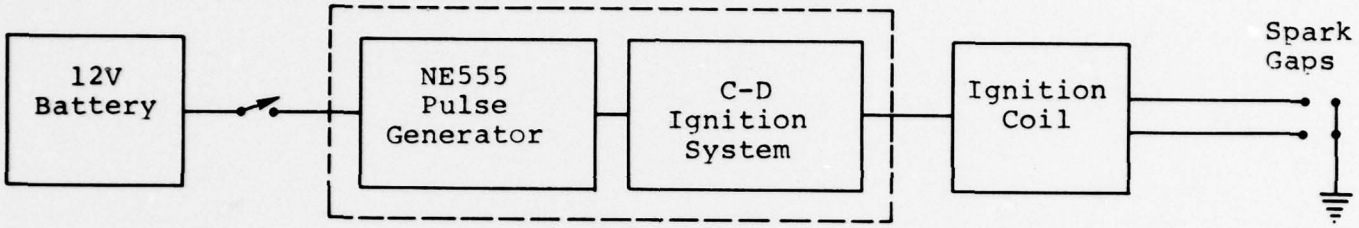

Figure 5. Block Diagram of Pulsing Circuit.

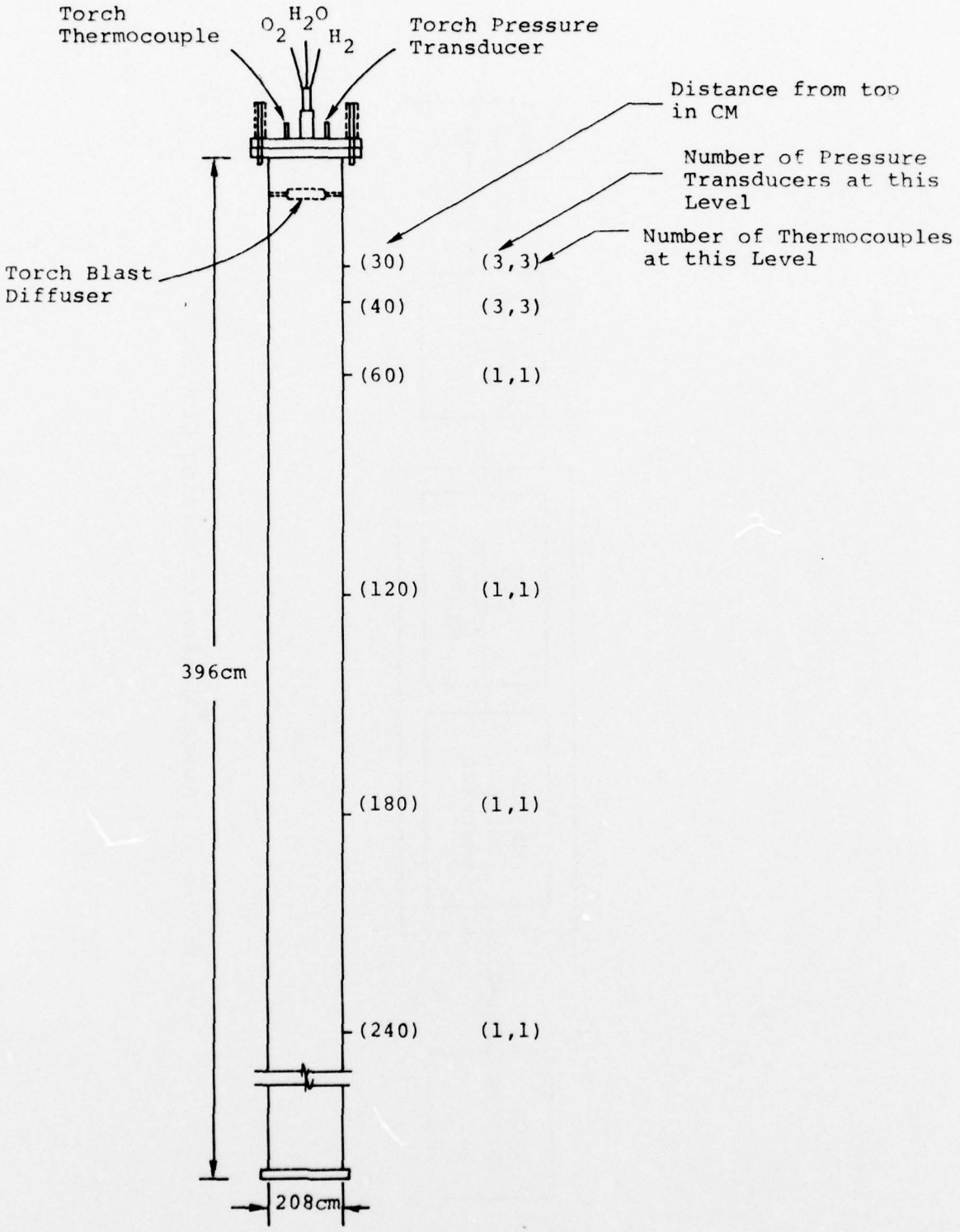

Figure 6. Drawing of Transite Pipe with Torch Flange Installed.

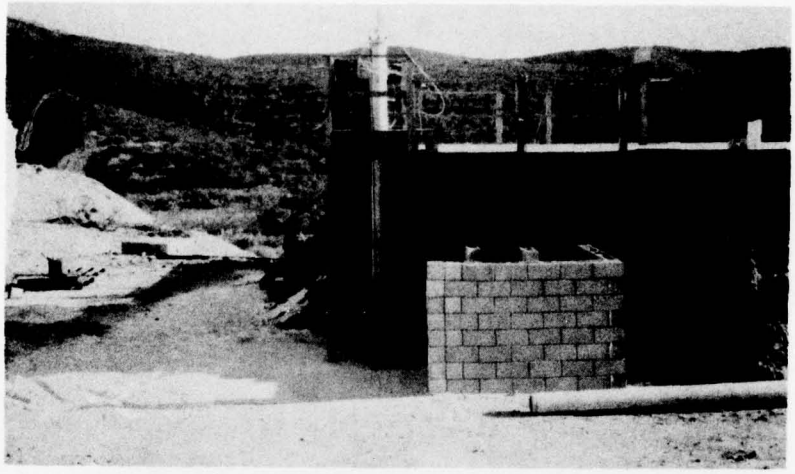

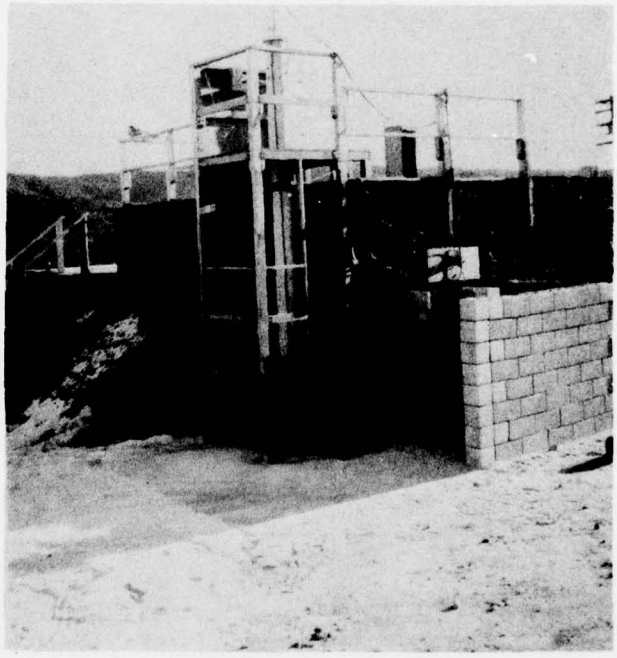

Figure 7. Test Pipe Mounted Alongside Control Bunker. Hydrogen and Oxygen Bottles are located behind block walls to right of test pipe.

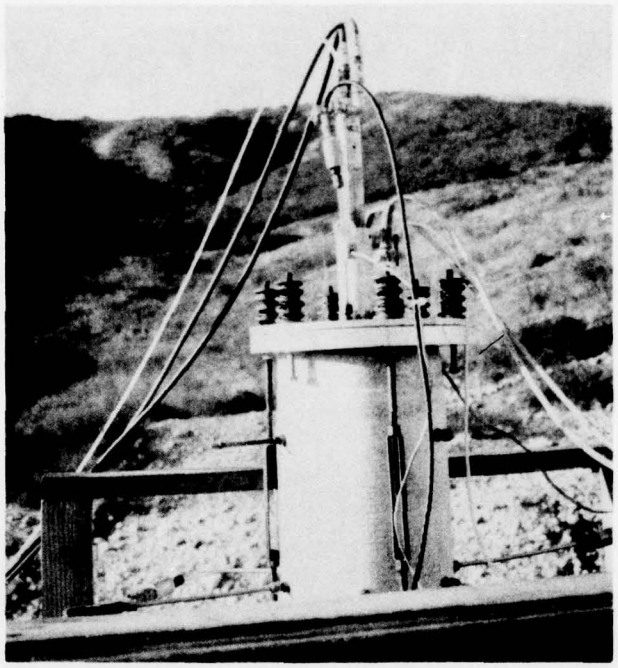

Figure 8. Torch Flange Mounted on Test Pipe. (Note: Pressure relief springs)

these rods the top and bottom flanges were forced tightly onto the pipe. During the course of the experiments, however, we discovered that the thermal expansion of the transite pipe was greater than could be accommodated by the iron rods. We, therefore, had to include a second set of springs in the system to allow expansion of the transite pipe. These are shown in Figure 9.

A blast deflector in the form of a ceramic fiber disk 7.5 cm in diameter by 2.5 cm thick was located approximately 7.5 cm below the torch tip and aligned with the torch axis. This ensured that the sand was not bored into by the steam cone.

Deflection of the steam cone caused severe ablation of the transite pipe and was responsible for catastrophic failure of at least one experiment. To eliminate this ablation, a cylindrical liner of ceramic fiber was fabricated and inserted into the combustion portion of the transite pipe. This liner was nominally 2.5 cm thick and possessed sufficient length to extend into the sand in the test chamber. After insertion of this liner, no further ablation problems were encountered.

In Figure 10 we show a picture of the ceramic fiber cylindrical liner as well as the ceramic fiber blast deflector. This photograph was taken immediately after a test had been run. Note that there is considerable spalling of liner. Note also that the spalling tends to occur along cylindrical surfaces in the liner. The significances of these cylindrical surfaces will be discussed in the following paragraphs.

After the initial experimentation period was completed and five successful data runs had been obtained, comparison

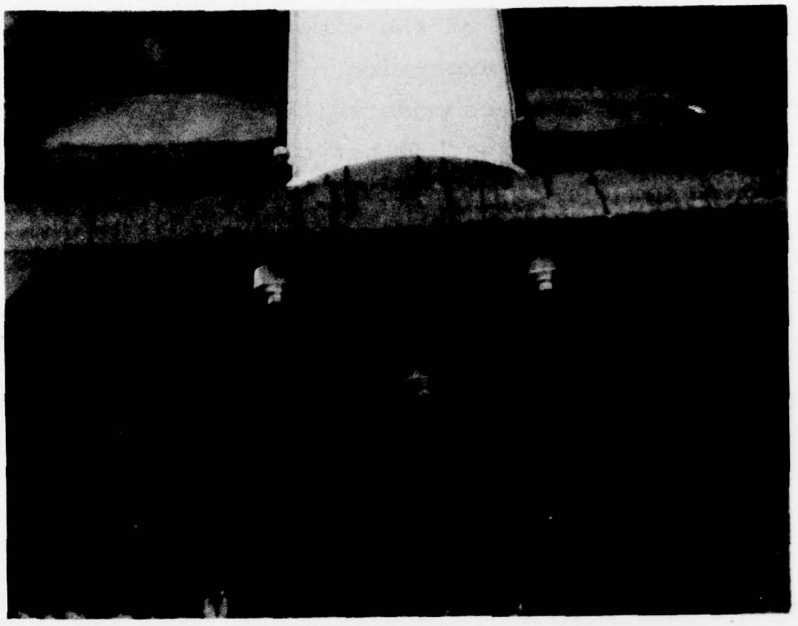

Figure 9. Pipe Expansion Springs Located at Bottom of Test Pipe.

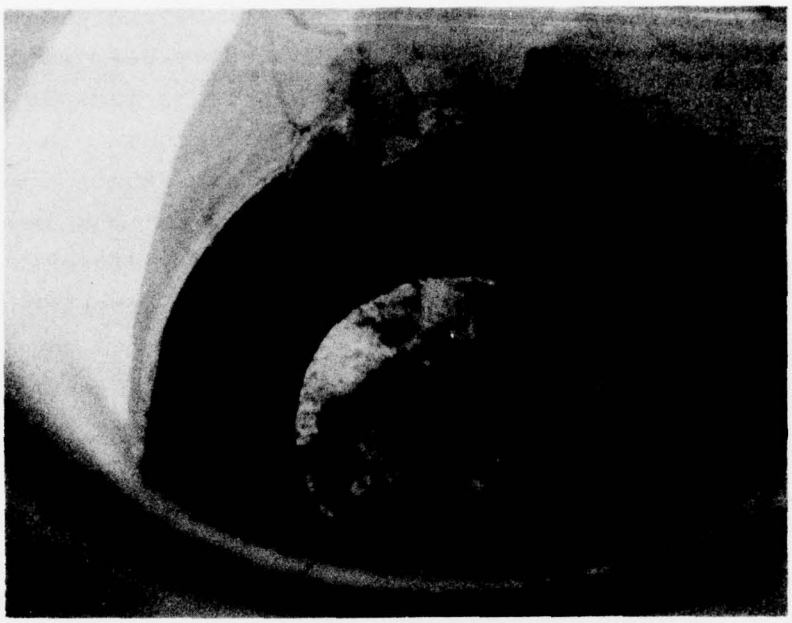

Figure 10. Blast Deflector and Lines Mounted in Test Pipe.

of measured data with theoretical expectations suggested that allowing the liner to extend into the sand may have caused a problem. This is because the liner possesses permeability in the axial direction due to the fact that it is made up of layers of woven fabric which are bonded together. In order to ascertain whether this effect is, in fact, what is seen in the data and to eliminate it, the sand level was lowered 5 cm beneath the bottom of the liner. Three additional experiments were undertaken much later in the experimental program. An extreme delay (almost six months) was encountered due to the record-breaking rains of Southern California.

The control and recording module was designed and fabricated to afford ease of operation and allow instantaneous assessment of the condition both of the torch and the conditions within the transite pipe. A picture of this is shown in Figure 11. A block diagram of the monitoring and recording system is presented in Figure 12. Pressures and temperatures along the transite pipe and within the combustion zone were monitored and continuously recorded and displayed during the course of each experiment.

Pressures were monitored using Sensometric transducers of appropriate ranges. These were mounted external to the transite pipe. Pressure communication was effected by means of 0.09 cm wall by 0.6 cm diameter stainless steel tubes which extended into the sand at the appropriate axial and radial locations. Pressure integrity was maintained by use of Swage-type feed-throughs inserted into transite pipe walls.

J-type thermocouples (iron vs. copper nickel) were mounted at similar axial and radial locations as the pressure transducers. Temperatures in the combustion zone were monitored by either a Tungsten-5% Rhenium vs. Tungsten-26%

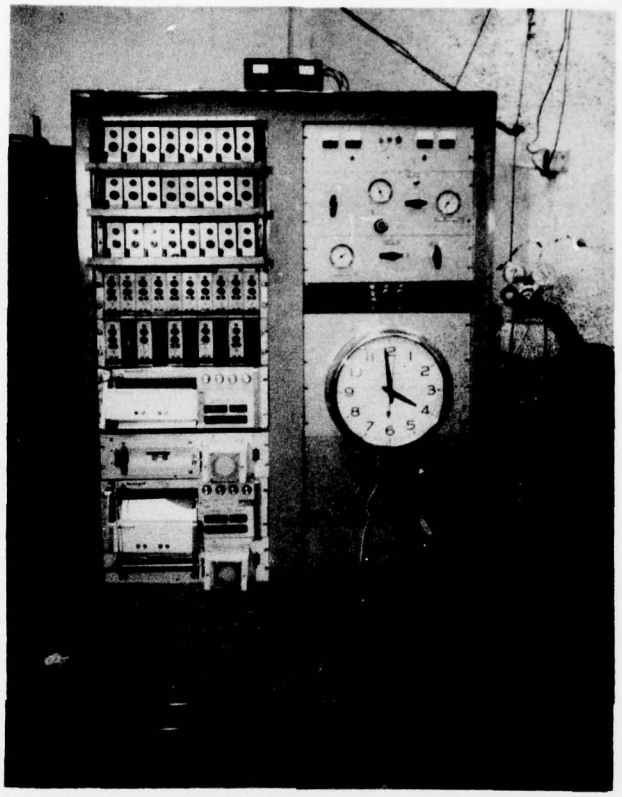

Figure 11. Control and Recording Module.

H_2 Torch

Block Diagrams of Monitoring/Recording Equipment

1. Pressure Monitoring (11 channels)

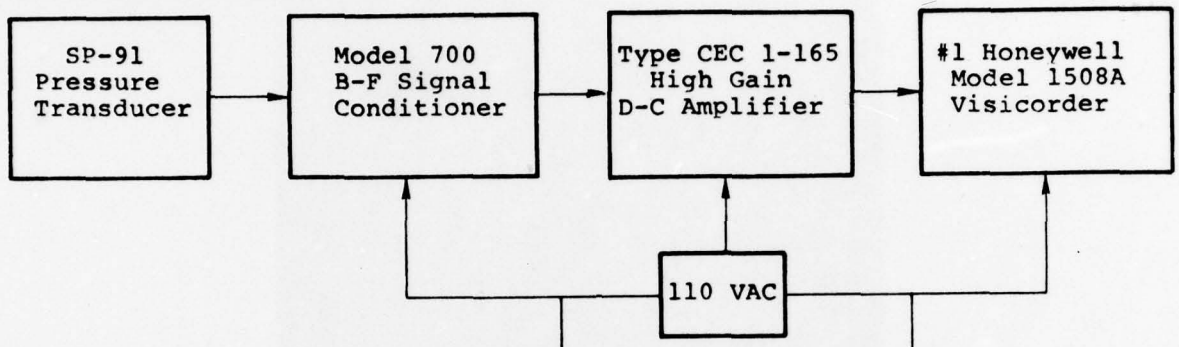

2. Temperature Monitoring (11 channels)

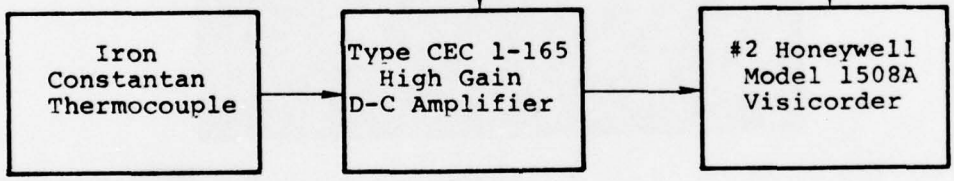

3. Water Flow to Nozzle (1 channel)

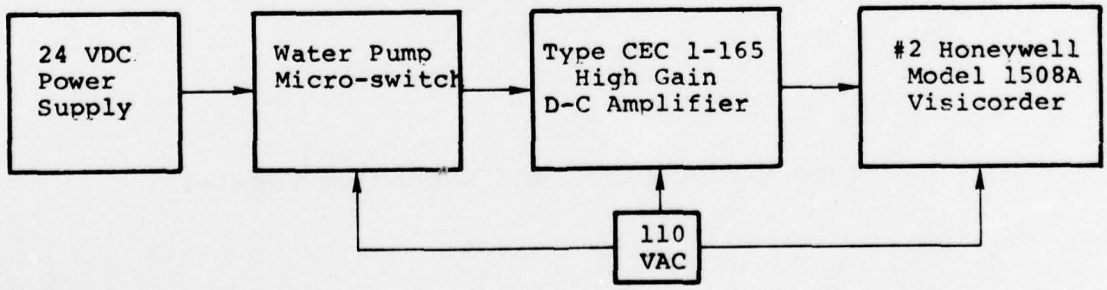

Figure 12. Block Diagram of Monitoring and Recording System.

Rhenium type or a K-type (Nickel-Chromium vs. Nickel Aluminum) thermocouple. All reference temperatures were nominally 80°F.

Water flow to the torch head was continuously monitored during the course of each experiment. The right hand side of the console shown in Figure 11 is devoted primarily to controlling both gas and water flow. A diagram of the water and combustible gas control systems is presented in Figure 13. Note that neither hydrogen nor oxygen are directly controlled from within the bunker. Instead, slave regulators controlled by nitrogen pressure provide control of delivery pressures from the hydrogen and oxygen bottles. In this way, combustible gases are never allowed to enter the enclosed region in which experimenters work. During the course of an experiment, nitrogen pressure to the slave regulators is under continuous control of the experimenter.

Delivery flows are further controlled by means of precision gas metering valves which have been previously calibrated utilizing flow of nitrogen gas under known conditions. Water is delivered by a gas driven positive displacement pump (Haskell Model MS-21). The flow rate is controlled by a precision metering valve. The water pump could deliver water flows of between 0 and 300 cc/min. By use of the three metering valves, it is possible to ensure that flows are in accord with the design flow rate for a particular experiment.

A block diagram of the nitrogen gas control system is shown in Figure 14. This system ensures that the experimenter could immediately interrupt the flow of hydrogen and oxygen to the system. In the event of a power failure during the course of the experiment, the gas control solenoid would open and interrupt the flow of hydrogen and oxygen to the torch.

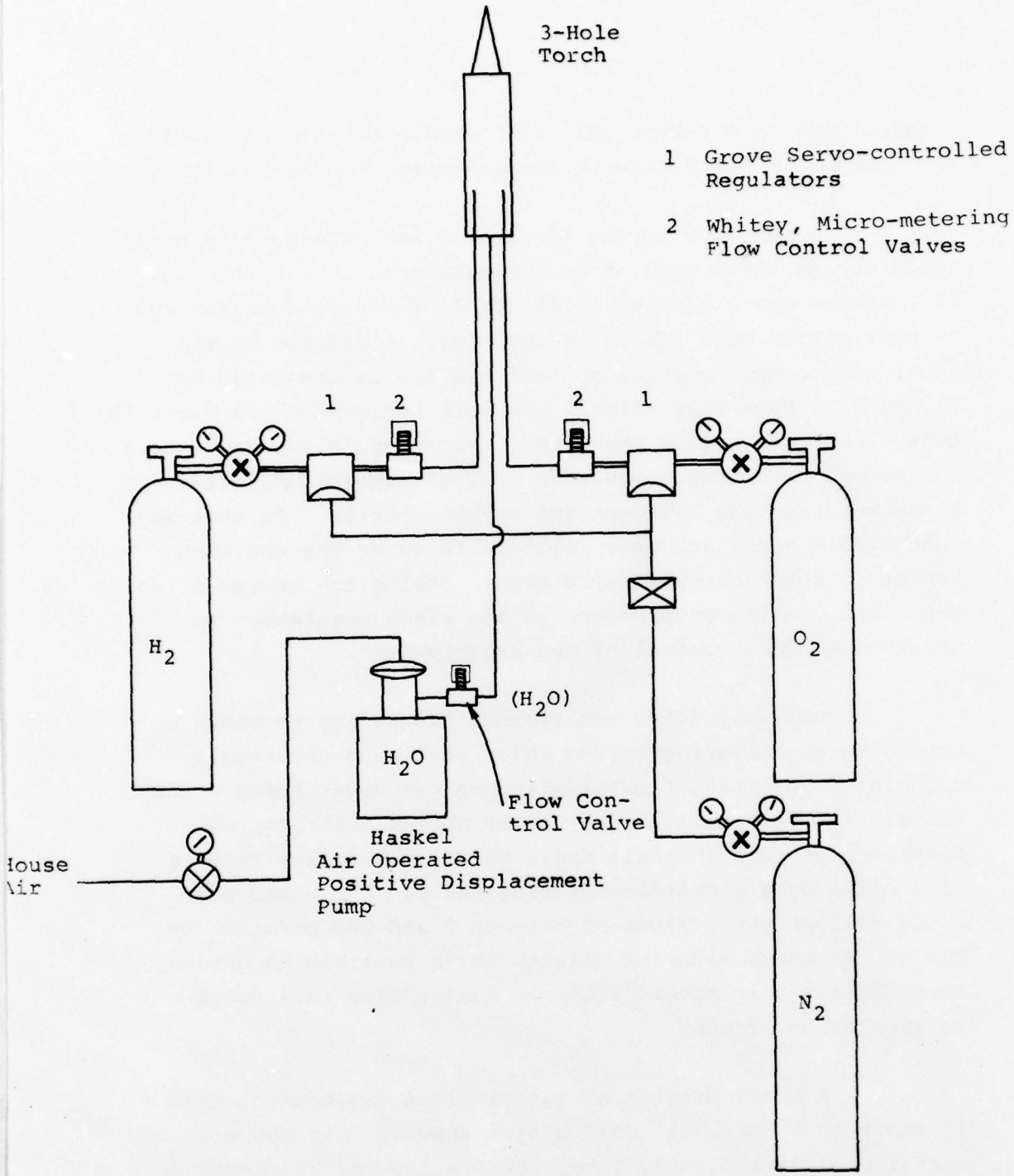

Figure 13. Water, Hydrogen, and Oxygen Control System.

H_2 Torch

Block Diagrams of Operating Systems (Electrical)

1. Ignition System

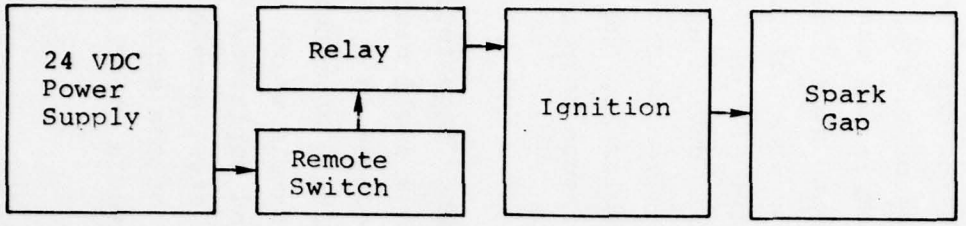

2. Gas Servo Control

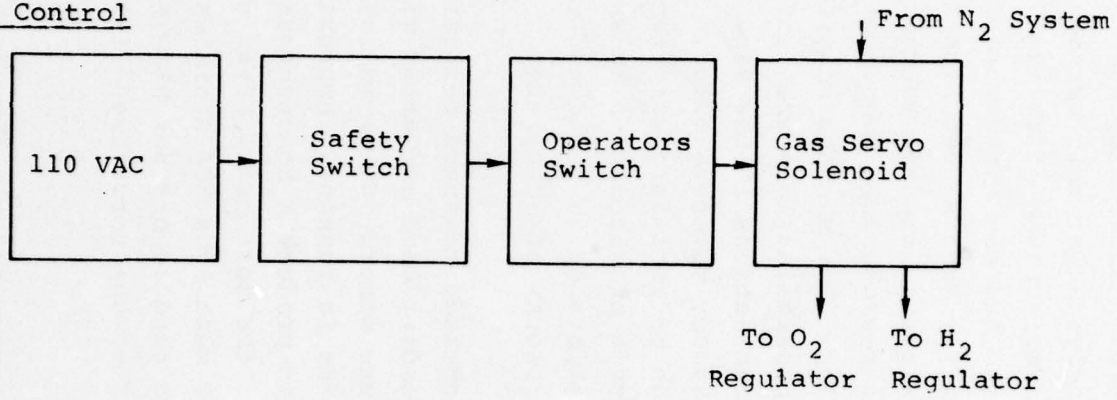

Figure 14. Nitrogen Gas Control System.

The test material utilized in the experiments is sixty mesh Overton sand. Representative chemical analyses and screen analyses for this particular sand are contained in Table 1. Emplacement of the sand in the test column was done by raining the sand into the pipe in a controlled fashion. Experience at the Nevada Test Site has indicated that the raining technique as opposed to tamping or vibrating is probably the most reproducible manner of emplacing sand in an enclosed region. The sand as shipped and stored is essentially dry, possessing moistures on the order of 0.1%. Moisture determinations in the sand were all performed utilizing a Speedy moisture meter. This device utilizes the generation of acetylene gas from wetted calcium carbide. The gas pressure produced in a known volume by the acetylene gas can be calibrated to yield the moisture required to produce that amount of acetylene.

Increased moisture content, when required, is obtained by blending sand and water with a small gasoline-driven concrete mixer. Water is introduced in a fine stream while the mixer is running. Approximately 30 minutes of mixing is required to produce a homogeneous sample which is then emplaced into the test bed. After sand emplacement, three layers of 100 mesh, type 304 stainless steel screen are placed on top of the sand to prevent blowing of the sand. Immediately thereafter the torch head fixture is attached to the test bed.

A compressed air flow test is performed prior to ignition. The need for a such test was not apparent initially. Consequently only the last third of the tests performed had flow measurements performed. The theory used to analyze the flow and equivalent permeabilities is contained in Appendix A2.

TABLE 1

PROPERTIES OF OVERTON SAND

REPRESENTATIVE CHEMICAL ANALYSES

	No.60
Silicon dioxide (SiO_2)	99.34 %
Iron oxide (Fe_2O_3)	0.063
Aluminum oxide (Al_2O_3)	0.27
Titanium dioxide (TiO_2)	0.043
Calcium oxide (CaO)	0.03
Magnesium oxide (MgO)	0.02
Sodium oxide (Na_2O)	0.04
Potassium oxide (K_2O)	None

REPRESENTATIVE SCREEN ANALYSES

	No.60
On 30 mesh	0.6 %
40	7.7
50	18.3
70	29.0
100	33.7
140	9.0
200	1.4
270	0.2
Pan	0.1
AFS	60

In addition to measurement of the temperature and pressures in the sand column, we were advised that the time of arrival of liquid water and/or saturation percentage are desirable quantities to measure. This is so because of the existence of several calculational codes which follow steam propagation. These codes do not generally agree on saturation levels. A straightforward way to monitor saturation is by observing the change in dielectric constant in a capacitor. As liquid water enters between the capacitor plates the mean dielectric constant of the materials between the plates changes markedly. This change in dielectric constant can be related to arrival of water and saturation percentage. During the course of these experiments a cylindrical capacitor was used to perform these dielectric constant measurements. A picture of one such cylindrical condenser is shown in Figure 15. Unfortunately, only two valid tests were performed with the cylindrical capacitors. Representative data from these two tests as well as the theory of the capacitive saturation gauge are contained in Appendix I.

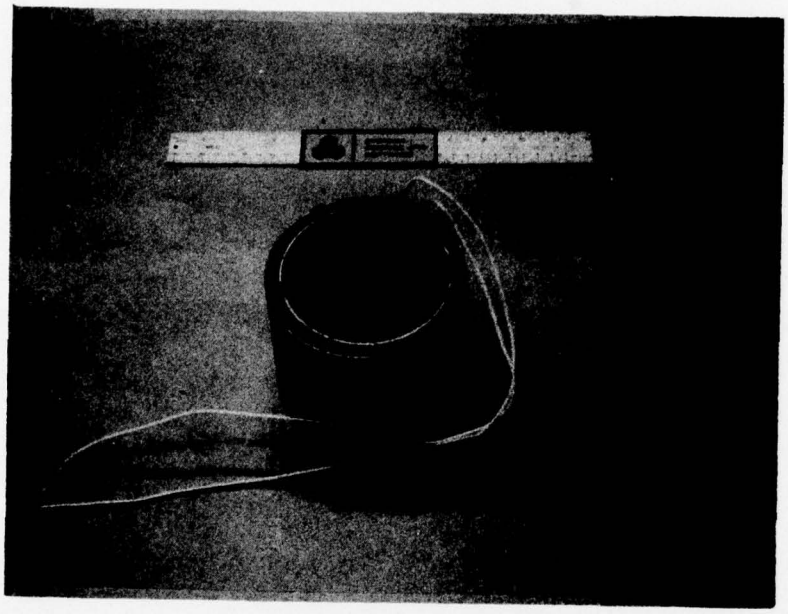

Figure 15. Cylindrical Capacitor used for Saturation Measurements.

IV. DATA

Nineteen experiments were attempted utilizing the hydrogen-oxygen steam-generating torch mounted on a sand filled column. Of these, eight experiments produced data which could be used for comparison with calculations. In this section, these data are presented along with the salient experimental parameters required for interpretation. Note that pressures are given in psi and temperatures are given in degrees centigrade.

EXPERIMENT I (8/11/77)

Total Mass Sand = 1.703×10^5 gm

Moisture (initial) = 0.1% (Dry)

Available Volume for Sand = 1.091×10^5 cc

ρ_{bulk} = 1.562 gm/cc

ϕ = 41%

S = 0.4%

Flow Input = 3 gm/sec Steam

Initial Permeability = not measured

T_1 is W-5% Rhenium vs. W-26% Rhenium Thermocouple

T_2-T_{10} are "J" Thermocouples

EXPERIMENT I (8/11/77)

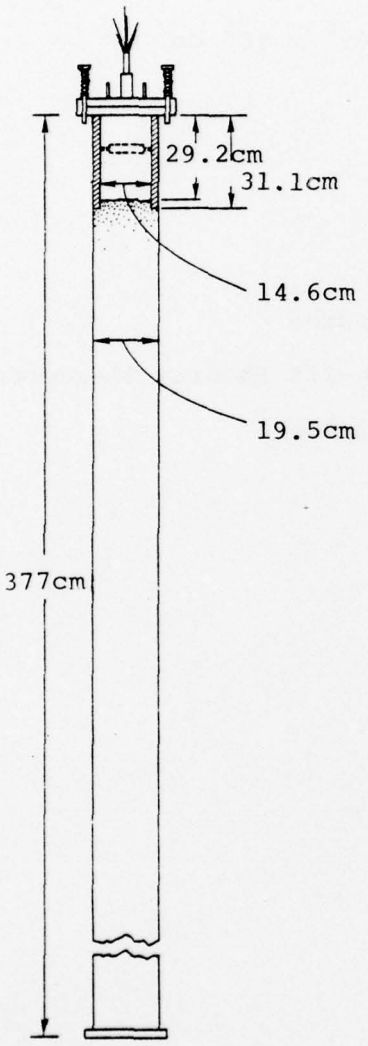

Transite Pipe

T_1 is Torch Diagnostic

Location (Below Sand)

T_2	3.1cm	1.25cm off center
T_3	3.1cm	2.5 cm off center
T_4	3.1cm	5.0 cm off center
T_5	13.1cm	1.25cm off center
T_6	13.1cm	2.5 cm off center
T_7	33.1cm	5.0 cm off center
T_8	33.1cm	1.25cm off center
T_9	92.5cm	1.25cm off center
T_{10}	FAILED	

P_1	is Torch Diagnostic	
P_2	3.1cm	1.25cm off center
P_3	3.1cm	2.5 cm off center
P_4	3.1cm	5.0 cm off center
P_5	13.1cm	1.25cm off center
P_6	13.1cm	2.5 cm off center
P_7	13.1cm	5.0 cm off center
P_8	33.1cm	1.25cm off center
P_9	92.5cm	1.25cm off center
P_{10}	FAILED	

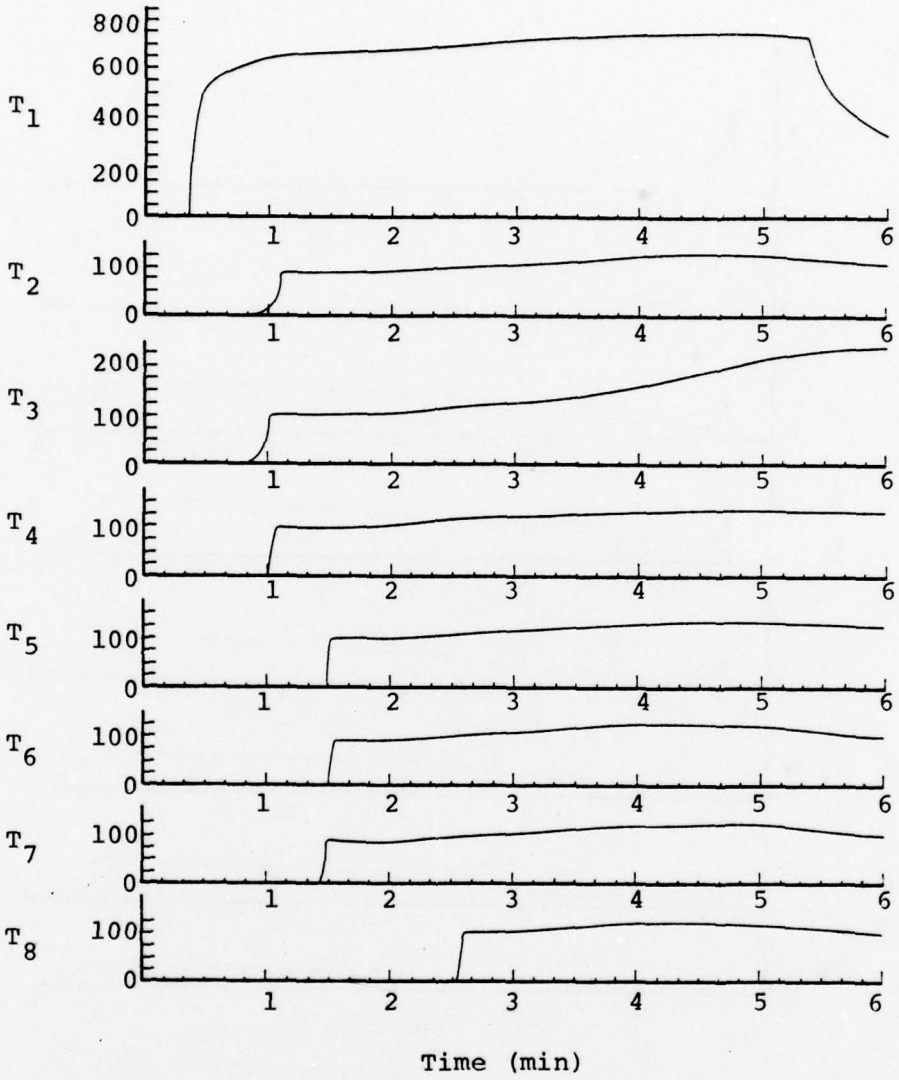

Temperature Versus Time for Experiment of 8/11/77.

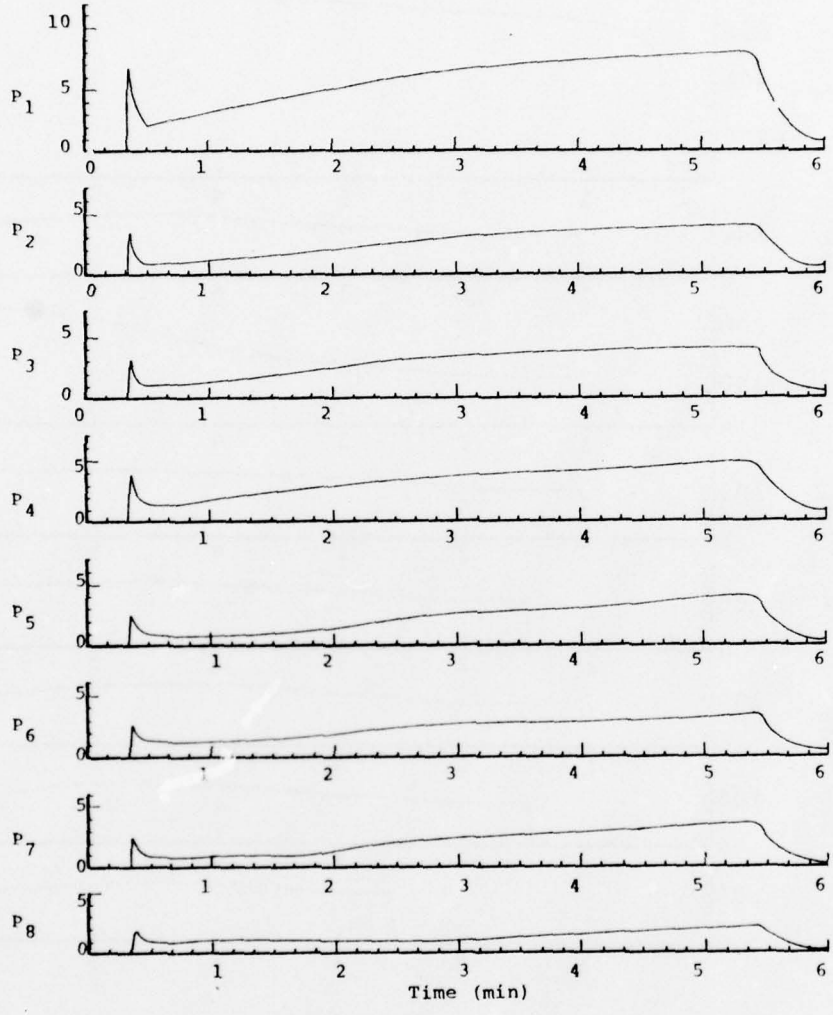

Pressure Versus Time for Experiment of 8/11/77.

EXPERIMENT II (8/19/77)

Total Mass Sand = 1.629×10^5 gm

Moisture (initial) = 3.3% (Dry)

Available Volume for Sand = 1.106×10^5cc

ρ_{bulk} = 1.473 gm/cc

ϕ = 44%

S = 11%

Flow Input = 3 gm/sec Steam

Initial Permeability = not measured

T_1 = W-5% Rhenium vs. W-26% Rhenium Thermocouple

T_2-T_{10} are "J" Thermocouples

EXPERIMENT II (8/19/77)

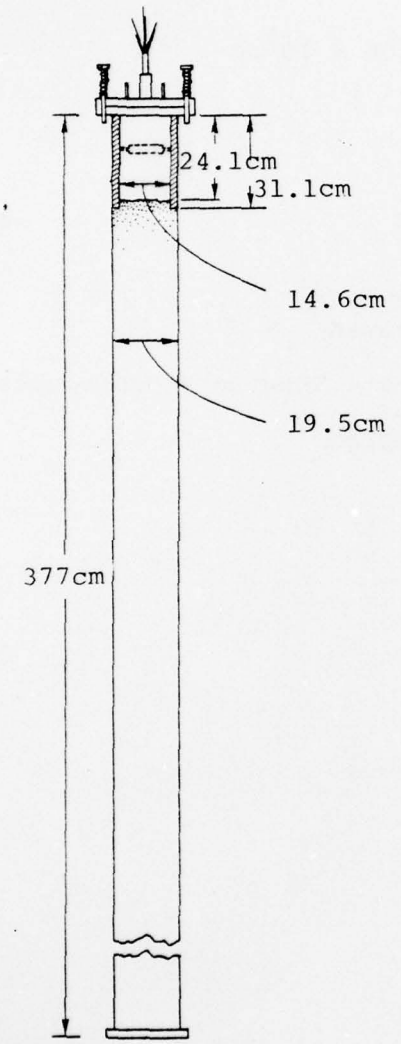

Transite Pipe

T_1 is torch diagnostic

Location (Below Sand)

T_2	3.1cm	1.25cm off center
T_3	3.1cm	2.5 cm off center
T_4	3.1cm	5.0 cm off center
T_5	13.1cm	1.25cm off center
T_6	13.1cm	2.5 cm off center
T_7	13.1cm	5.0 cm off center
T_8	33.1cm	1.25cm off center
T_9	92.5cm	1.25cm off center

P_1 is torch diagnostic

P_2	3.1cm	1.25cm off center
P_3	3.1cm	2.5 cm off center
P_4	3.1cm	5.0 cm off center
P_5	13.1cm	1.25cm off center
P_6	13.1cm	2.5 cm off center
P_7	13.1cm	5.0 cm off center
P_8	33.1cm	1.25cm off center
P_9	92.5cm	1.25cm off center

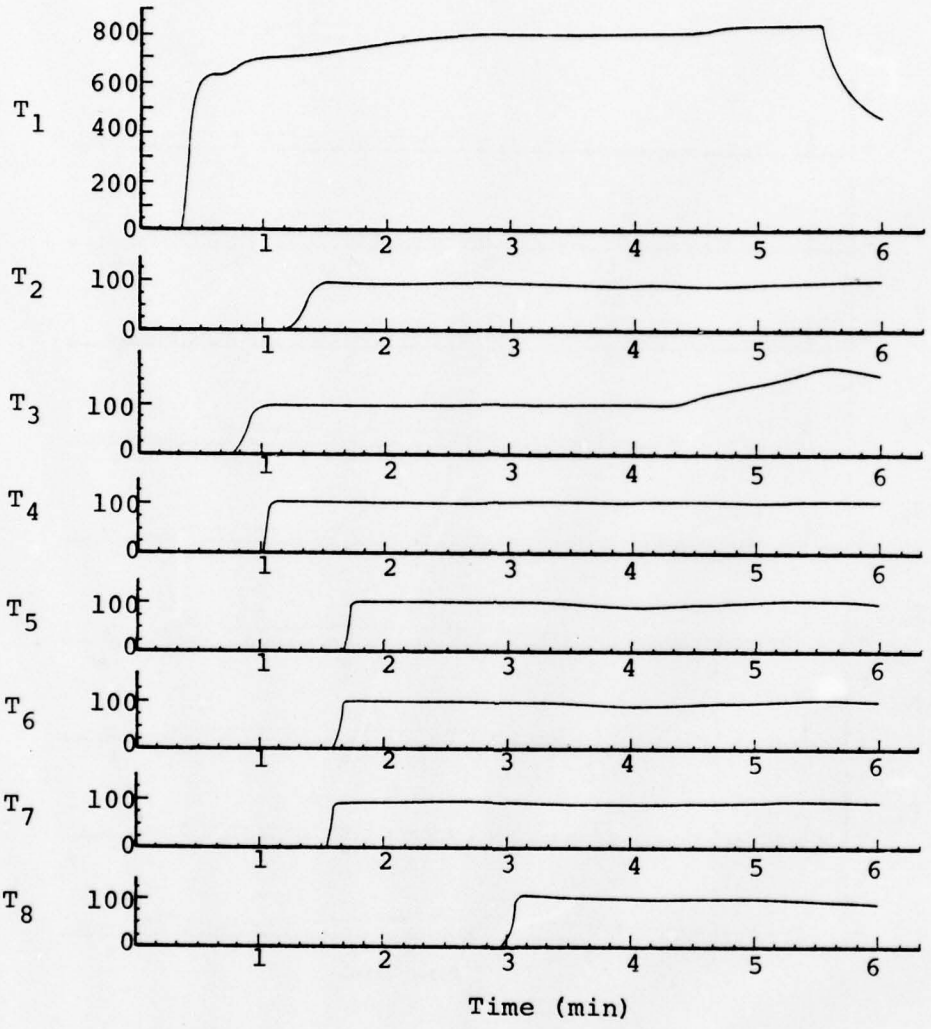

Temperature Versus Time for Experiment of 8/19/77.

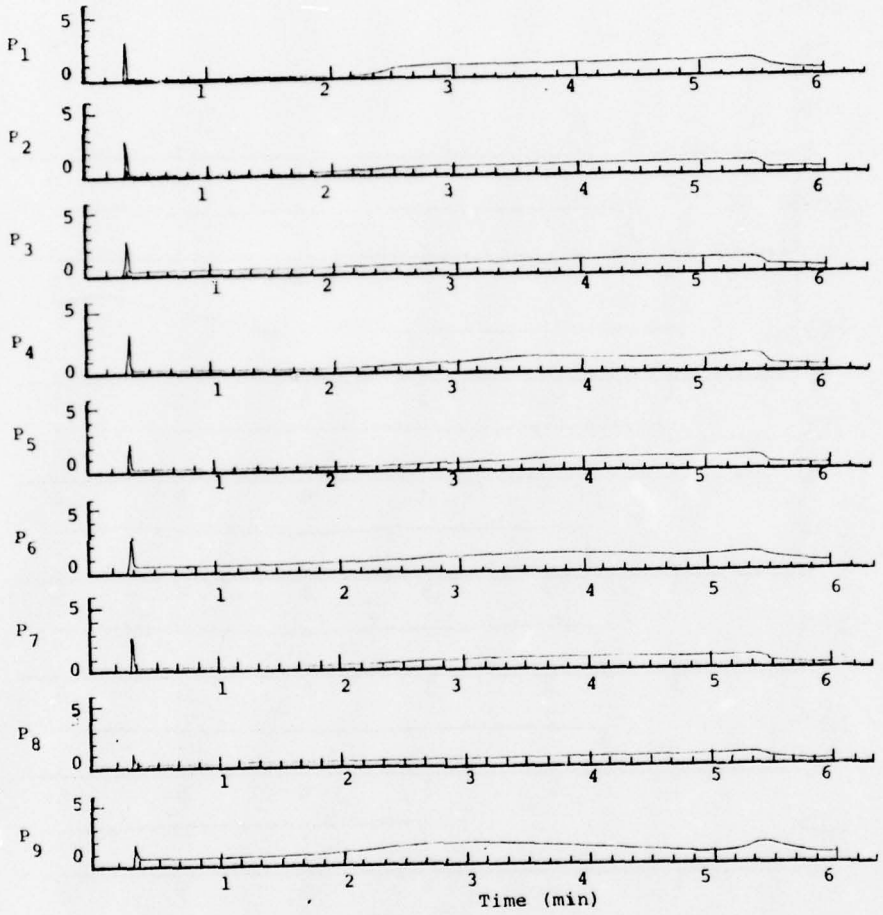

Pressure Versus Time for Experiment of 8/19/77.

EXPERIMENT III (8/24/77)

Total Mass Sand = 1.772×10^5 gm

Moisture (initial) = 0.2% (Dry)

Available Volume for Sand = 1.106×10^5 cc

ρ_{bulk} = 1.602 gm/cc

ϕ = 40%

S = 0.8%

Flow Input = 9 gm/sec Steam

Initial Permeability =

T_1 is K Thermocouple

T_2-T_9 are "J" Thermocouples

Note: outside of pipe hot to 146cm below sand after test.

EXPERIMENT III (8/24/77)

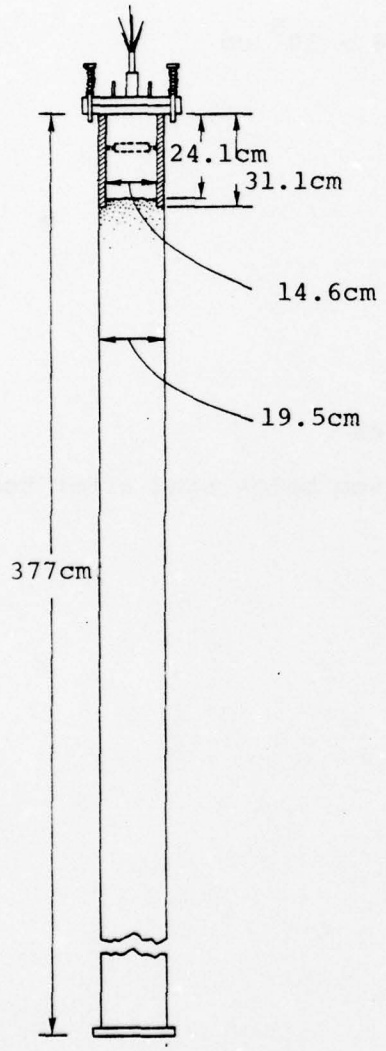

Transite Pipe

T_1 is torch diagnostic

Location (Below Sand)

T_2	6.9cm	1.25cm off center
T_3	6.9cm	2.5 cm off center
T_4	6.9cm	5.0 cm off center
T_5	16.9cm	1.25cm off center
T_6	16.9cm	2.5 cm off center
T_7	16.9cm	5.0 cm off center
T_8	36.9cm	1.25cm off center
T_9	16.9cm	on inside wall

P_1 is torch diagnostic

P_2	6.9cm	1.25cm off center
P_3	6.9cm	2.5 cm off center
P_4	6.9cm	5.0 cm off center
P_5	16.9cm	1.25cm off center
P_6	16.9cm	2.5 cm off center
P_7	16.9cm	5.0 cm off center
P_8	36.9cm	1.25cm off center
P_9	96.9cm	1.25cm off center

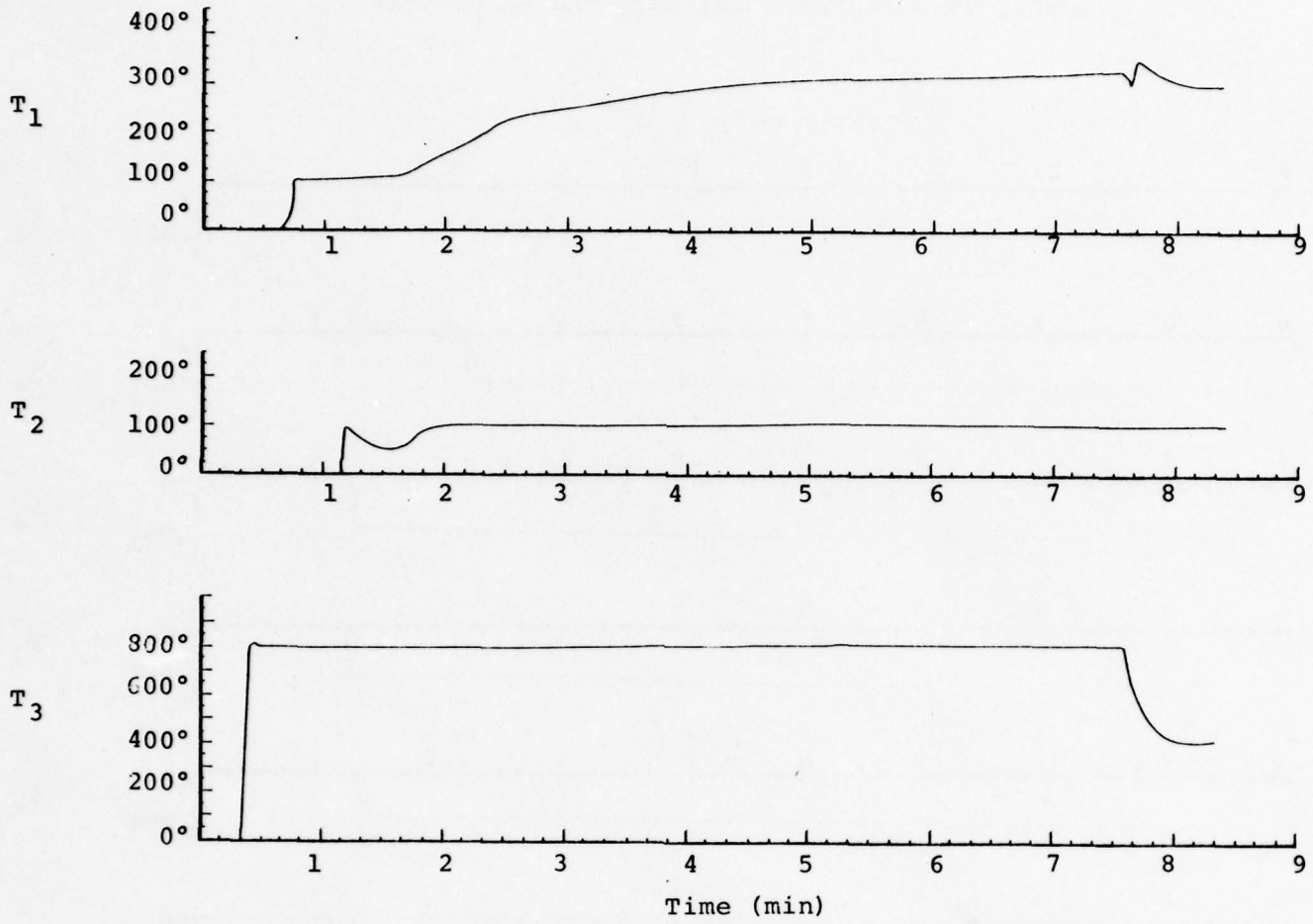

Temperature Versus Time for Experiment of 8/24/77.

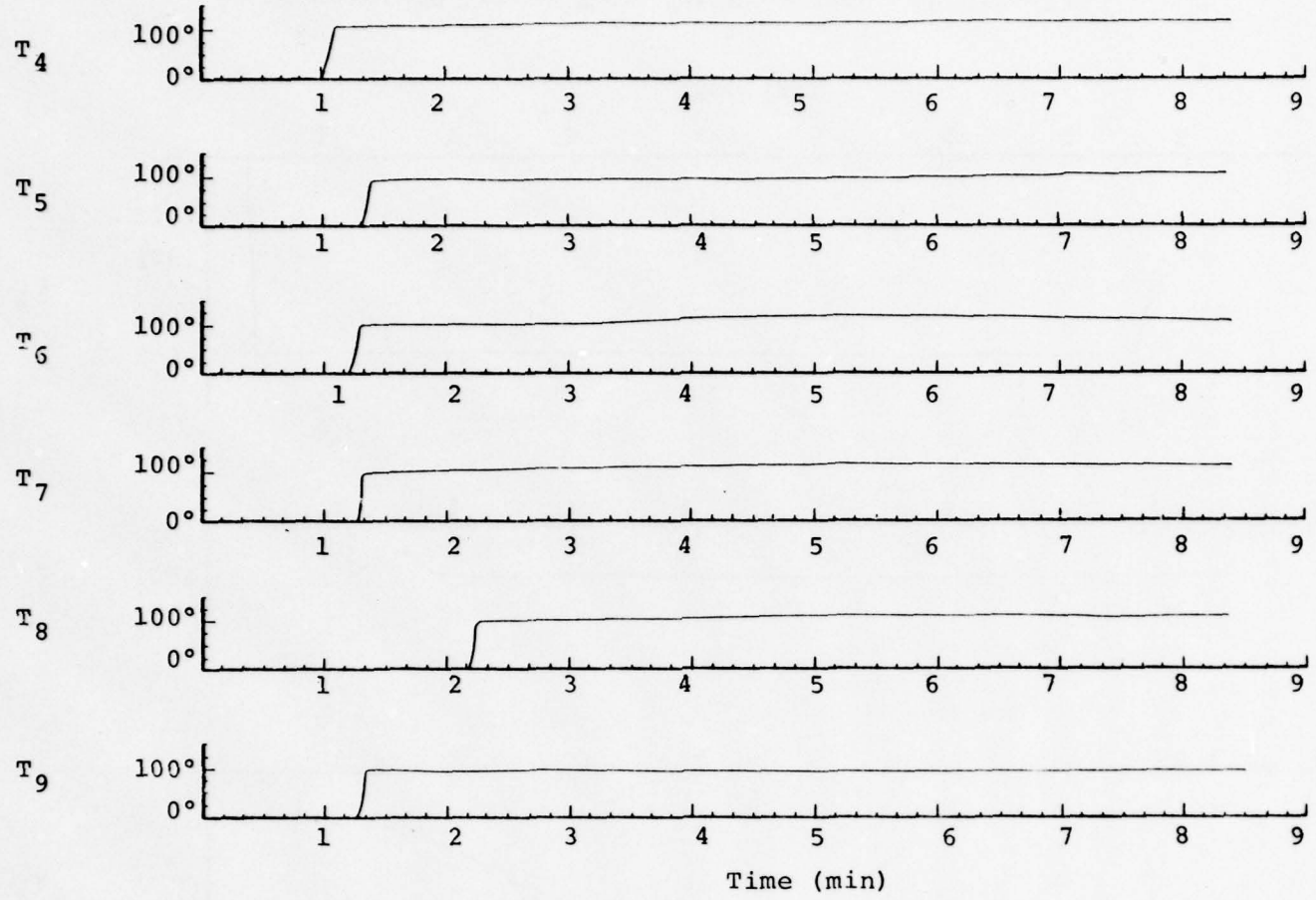

Temperature Versus Time for Experiment of 8/24/77.

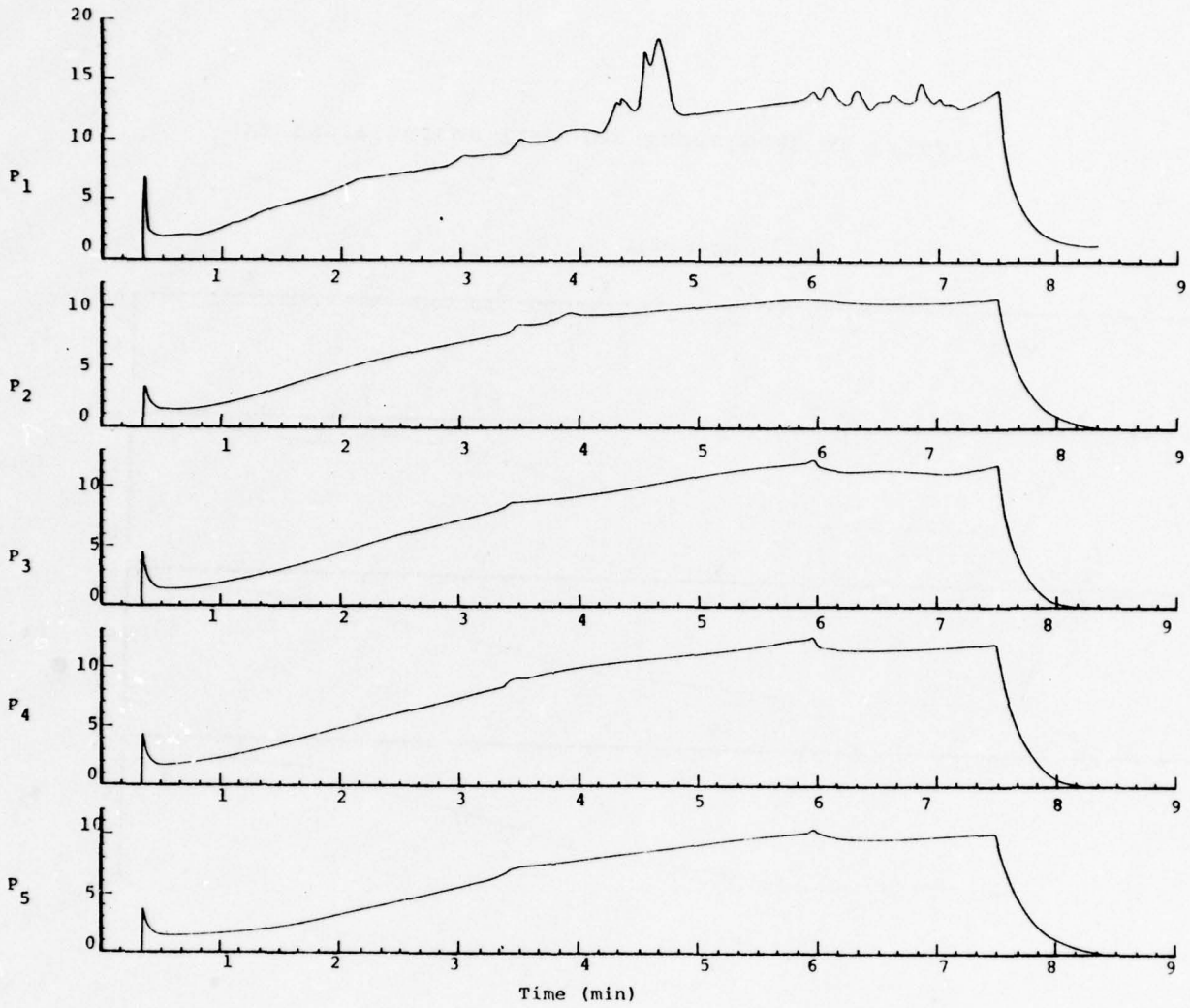

Pressure Versus Time for Experiment of 8/24/77.

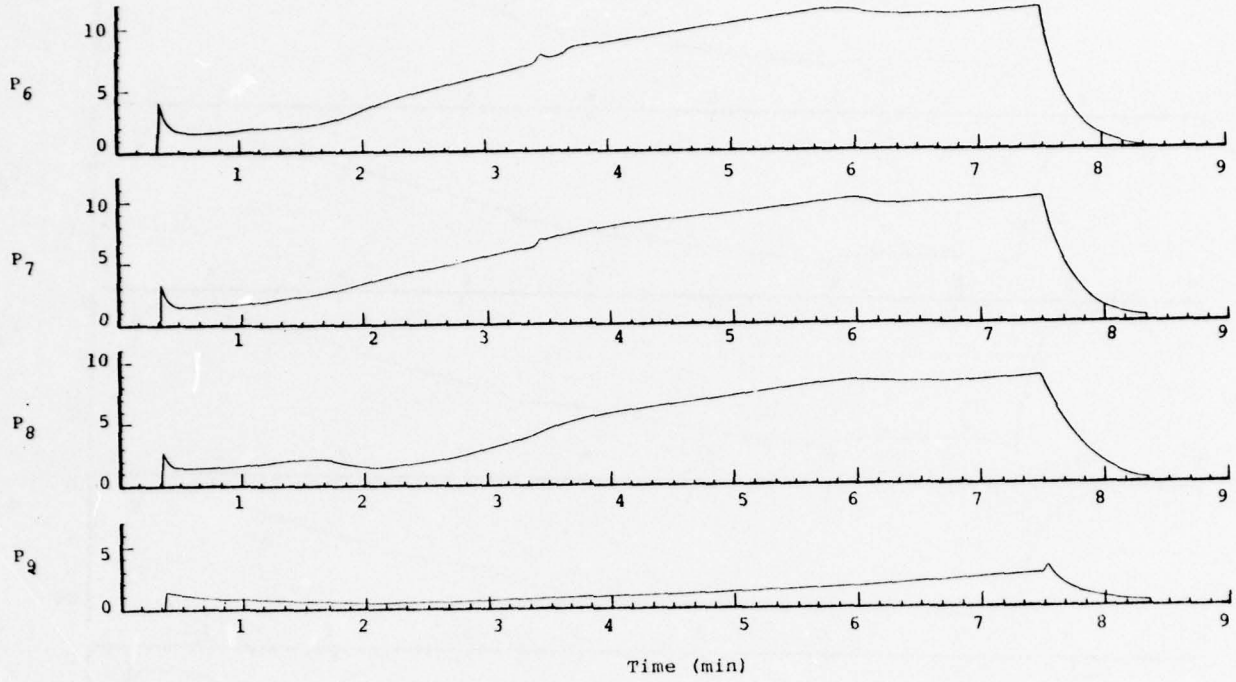

Pressure Versus Time for Experiment of 8/24/77.

EXPERIMENT IV (8/30/77)

Total Mass Sand = 1.748×10^5 gm

Moisture (initial) = 0.1% (Dry)

Available Volume for Sand = 1.062×10^5 cc

ρ_{bulk} = 1.646 gm/cc

ϕ = 38%

S = 0.4%

Flow Input = 6 gm/sec Steam

Initial Permeability = 42 darcy (measured)

T_1 is "K" Thermocouple

T_2-T_9 are "J" Thermocouples

Note: outside of pipe hot to 122cm below sand surface after test.

EXPERIMENT IV (8/30/77)

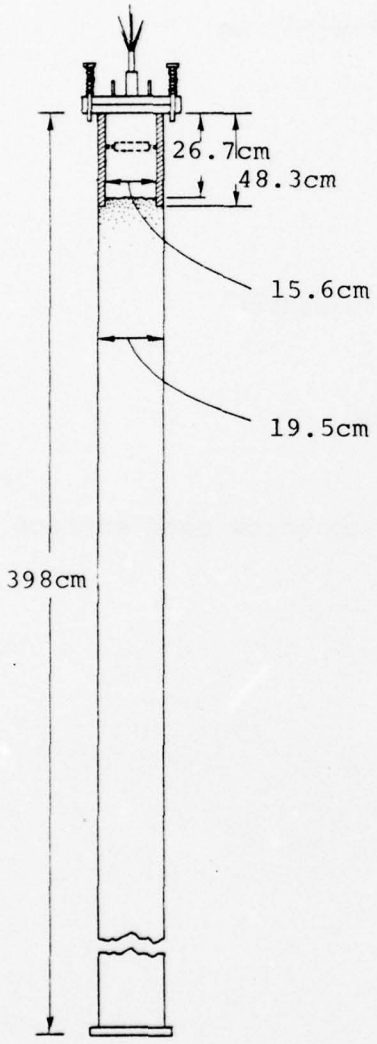

Transite Pipe

T_1 is torch diagnostic

Location (Below Sand)

T_2	5.9cm	1.25cm off center
T_3	6.9cm	2.5 cm off center
T_4	5.6cm	5.0 cm off center
T_5	15.9cm	1.25cm off center
T_6	17.3cm	2.5 cm off center
T_7	15.7cm	5.0 cm off center
T_8	36.6cm	1.25cm off center
T_9	17.6cm	(inside on wall)

P_1 is torch diagnostic

P_2	5.8cm	1.25cm off center
P_3	5.6cm	2.5 cm off center
P_4	5.9cm	5.0 cm off center
P_5	17.0cm	1.25cm off center
P_6	17.3cm	1.25cm off center
P_7	16.4cm	1.25cm off center
P_8	36.9cm	1.25cm off center

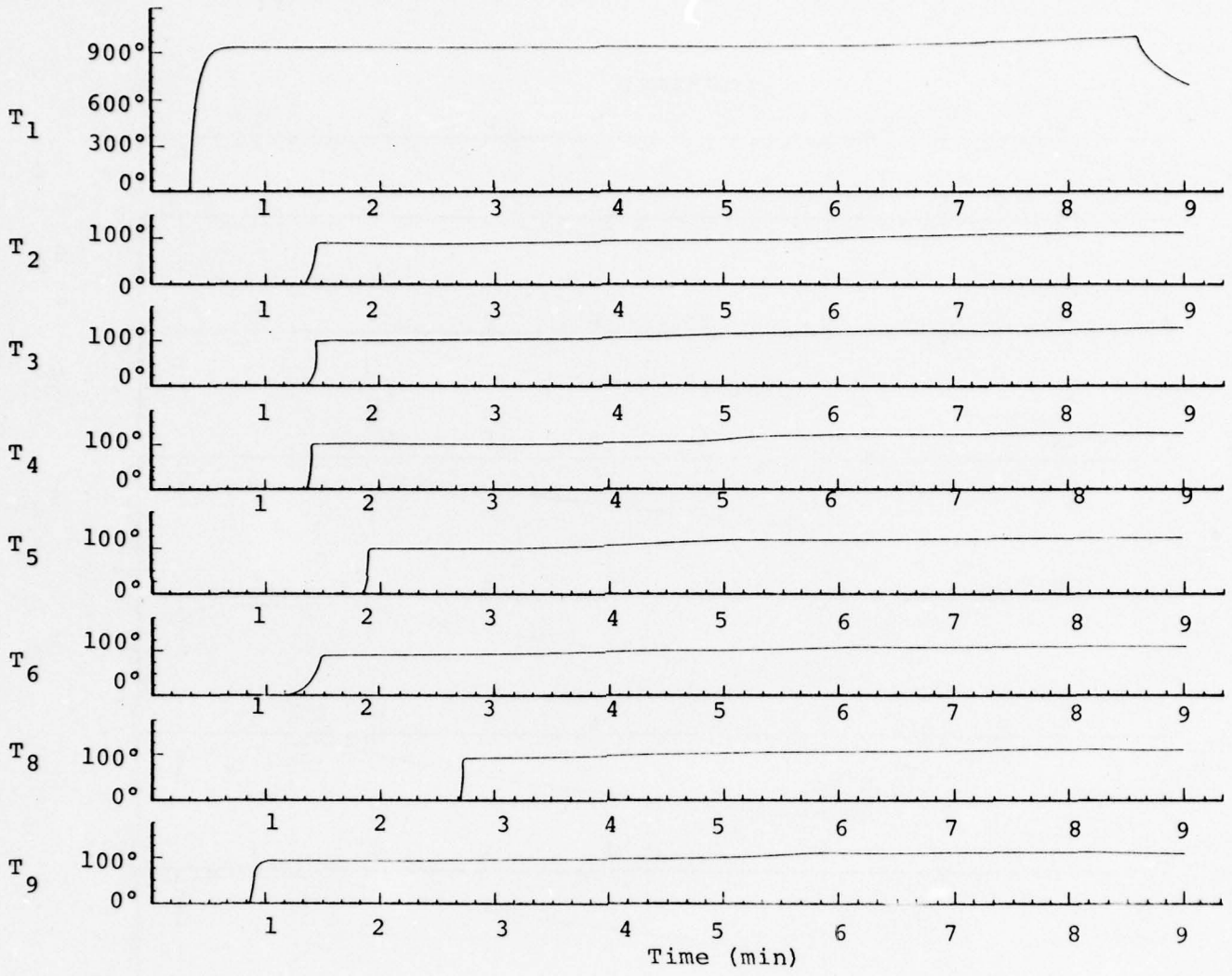

Temperature Versus Time for Experiment of 8/30/77.

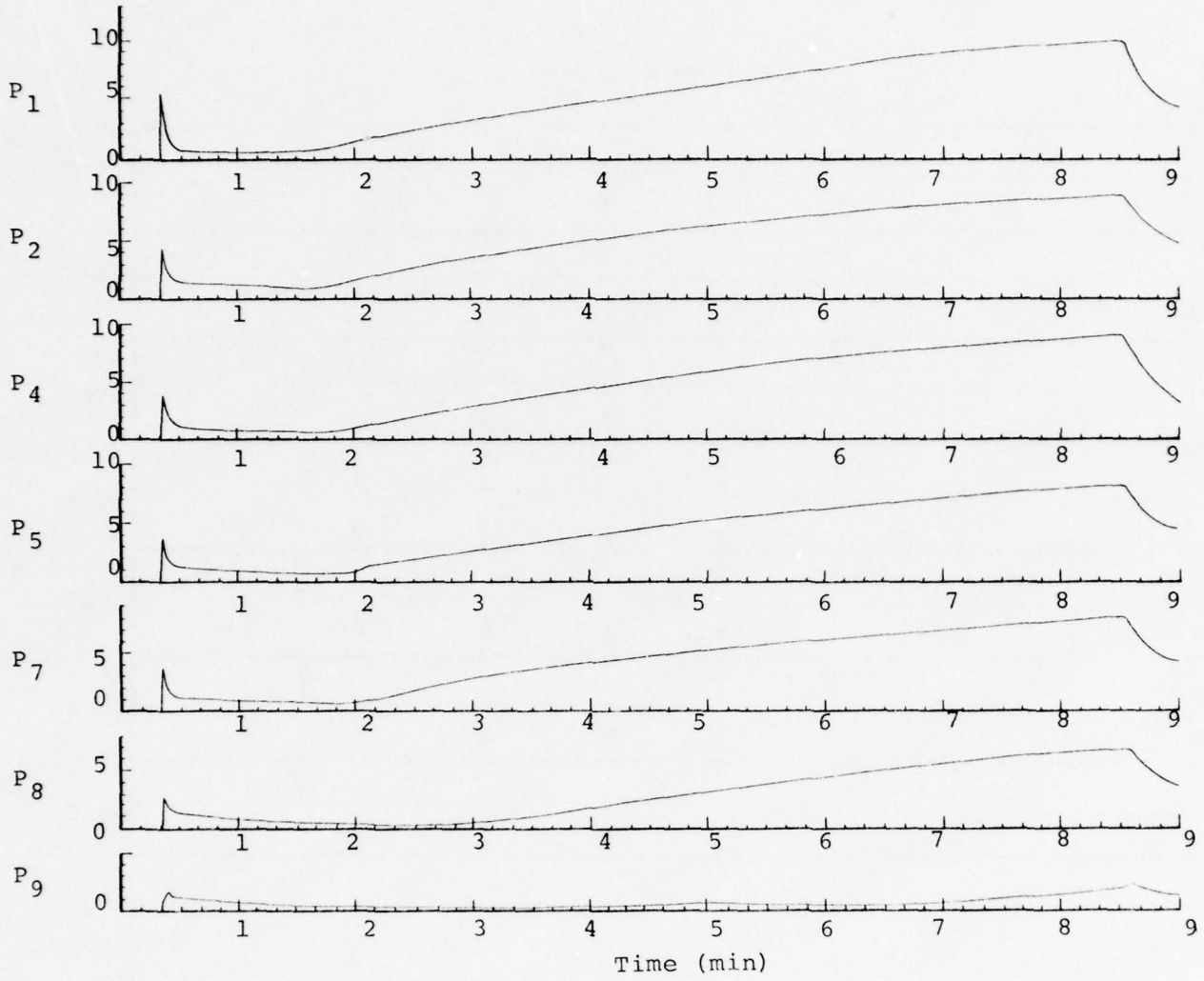

Pressure Versus Time for Experiment of 8/30/77.

Experiment V (11/2/77)

Total Mass Sand = 1.601×10^5 gm

Moisture (initial) = 2.2% (Dry)

Available Volume for Sand = 1.117×10^5 cc

ρ_{bulk} = 1.433 gm/cc

ϕ = 46%

S = 6.7%

Flow Input = 6 gm/sec Steam

Initial Permeability = 72 darcy (measured)

T_1 is "K" Thermocouple

T_2-T_{11} are "J" Thermocouples

Note: outside of pipe hot to 167cm below top of pipe after test.

EXPERIMENT V (11/2/77)

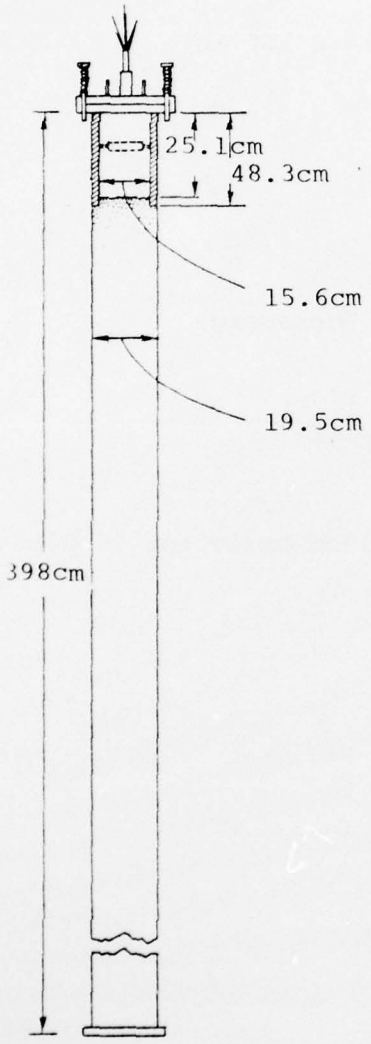

Transite Pipe

T_1 is torch diagnostic

Location (Below Sand)

T_2	7.8cm	1.25cm off center
T_3	8.4cm	3.75cm off center
T_4	7.3cm	8.75cm off center
T_5	19.1cm	1.25cm off center
T_6	18.4cm	3.75cm off center
T_7	18.6cm	8.75cm off center
T_8	18.3cm	1.25cm off center
T_9	57.3cm	1.25cm off center
T_{10}	77.2cm	1.25cm off center
T_{11}	95.9cm	1.25cm off center

P_1 is torch diagnostic

P_2	7.7cm	1.25cm off center
P_3	8.8cm	3.75cm off center
P_4	8.0cm	8.75cm off center
P_5	18.8cm	1.25cm off center
P_6	19.1cm	3.75cm off center
P_7	18.0cm	8.75cm off center
P_8	28.8cm	1.25cm off center
P_9	57.7cm	1.25cm off center

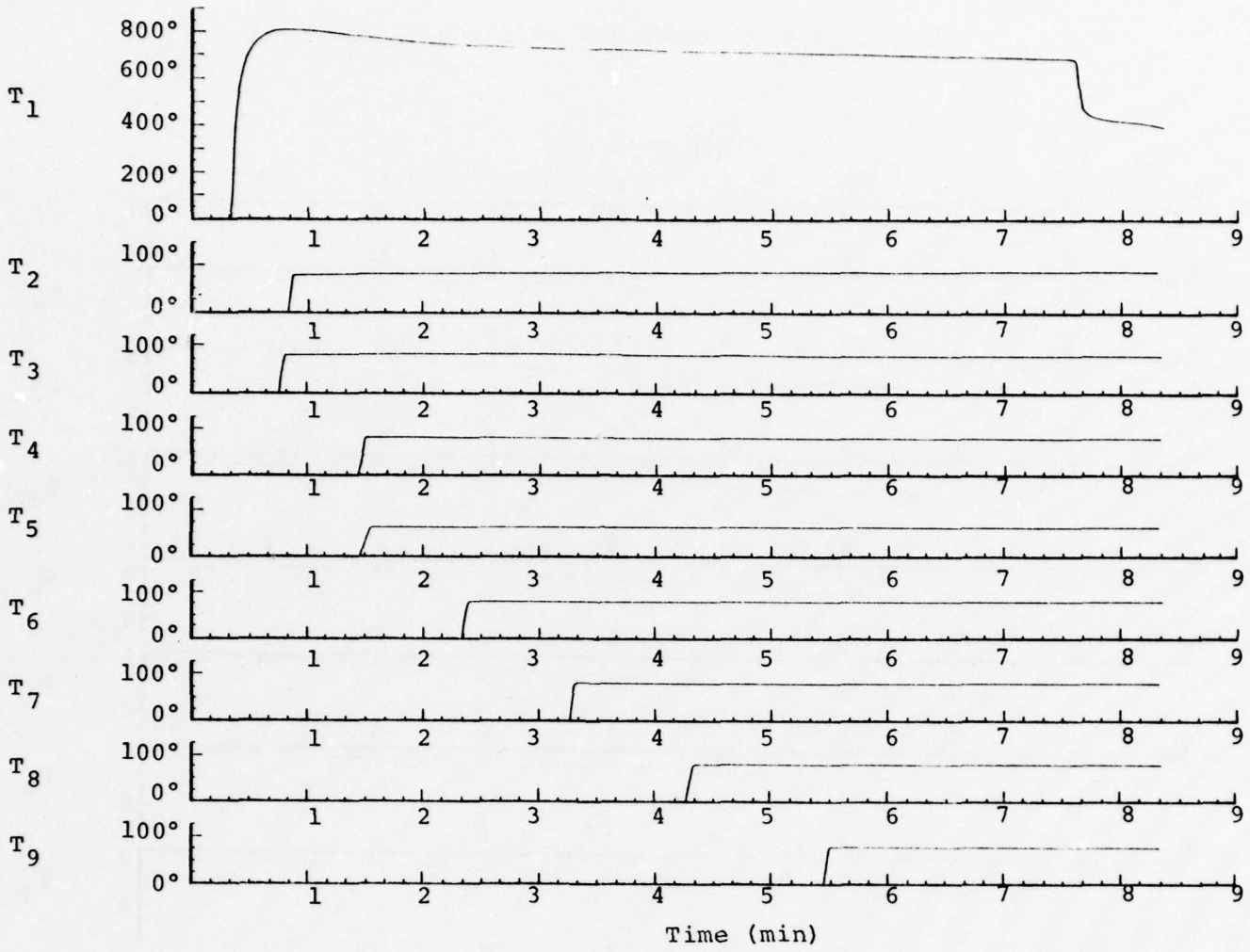

Temperature Versus Time for Experiment of 11/2/77.

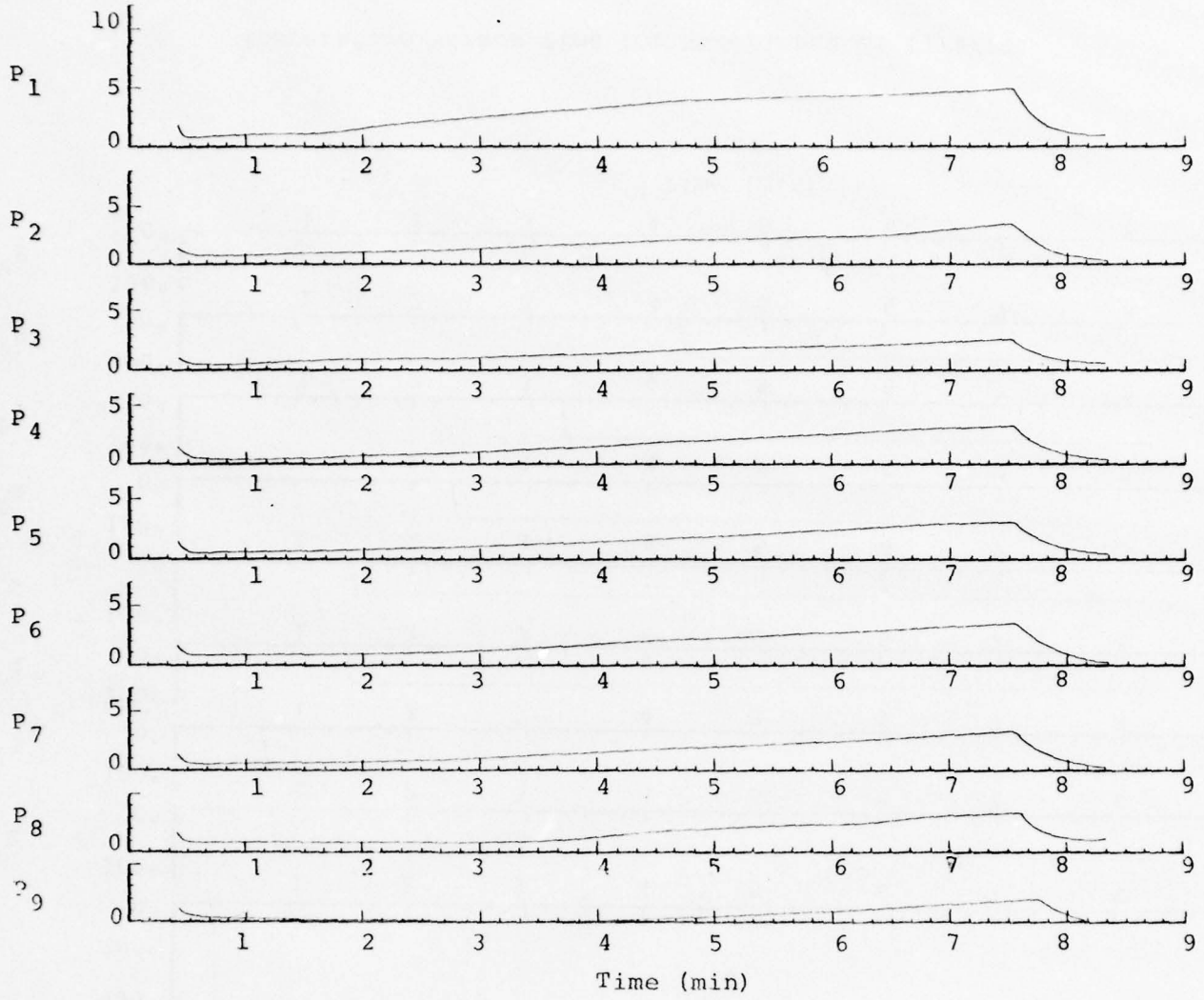

Pressure Versus Time for Experiment of 11/2/77.

EXPERIMENT VI (4/19/78)

Total Mass Sand = 1.650×10^5 gm

Moisture (initial) = 0.052 (Dry)

Available Volume for Sand = 1.038×10^5 cc

ρ_{bulk} = 1.590 gm/cc

ϕ = 40%

S = 0.2%

Flow Input = 6 gm/sec Steam.

Initial Permeability = 25 darcy (measured)

T_1 is "K" Thermocouple

T_2-T_8 are "J" Thermocouples

Note: At conclusion of test, outside of pipe hot to 142cm below top of pipe.

EXPERIMENT VI (4/19/78)

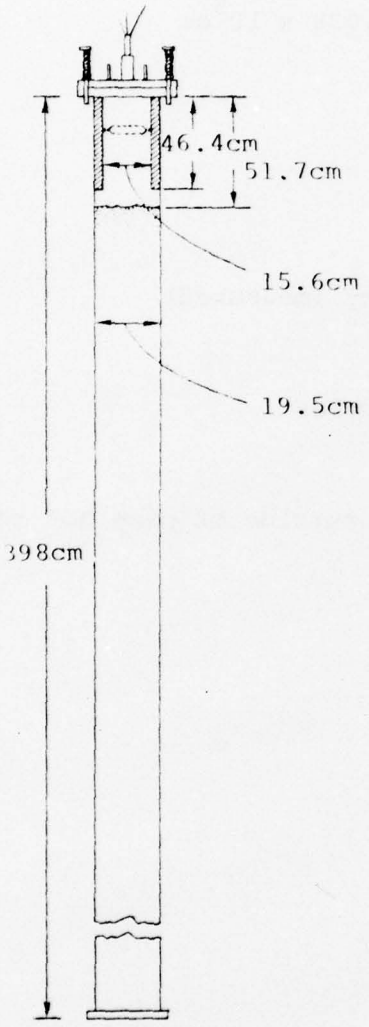

Transite Pipe

T_1 is torch diagnostic

Location (Below Sand)

T_2	5.6cm	5.0 cm off center
T_3	5.5cm	1.25cm off center
T_4	12.6cm	5.0 cm off center
T_5	12.6cm	1.25cm off center
T_6	31.4cm	1.25cm off center
T_7	51.5cm	1.25cm off center
T_8	72.0cm	1.25cm off center

P_1 is torch diagnostic

P_2	5.4cm	5.0 cm off center
P_3	5.3cm	1.25cm off center
P_4	12.4cm	5.0 cm off center
P_5	12.6cm	1.25cm off center
P_6	32.0cm	1.25cm off center
P_7	51.4cm	1.25cm off center
P_8	72.1cm	1.25cm off center

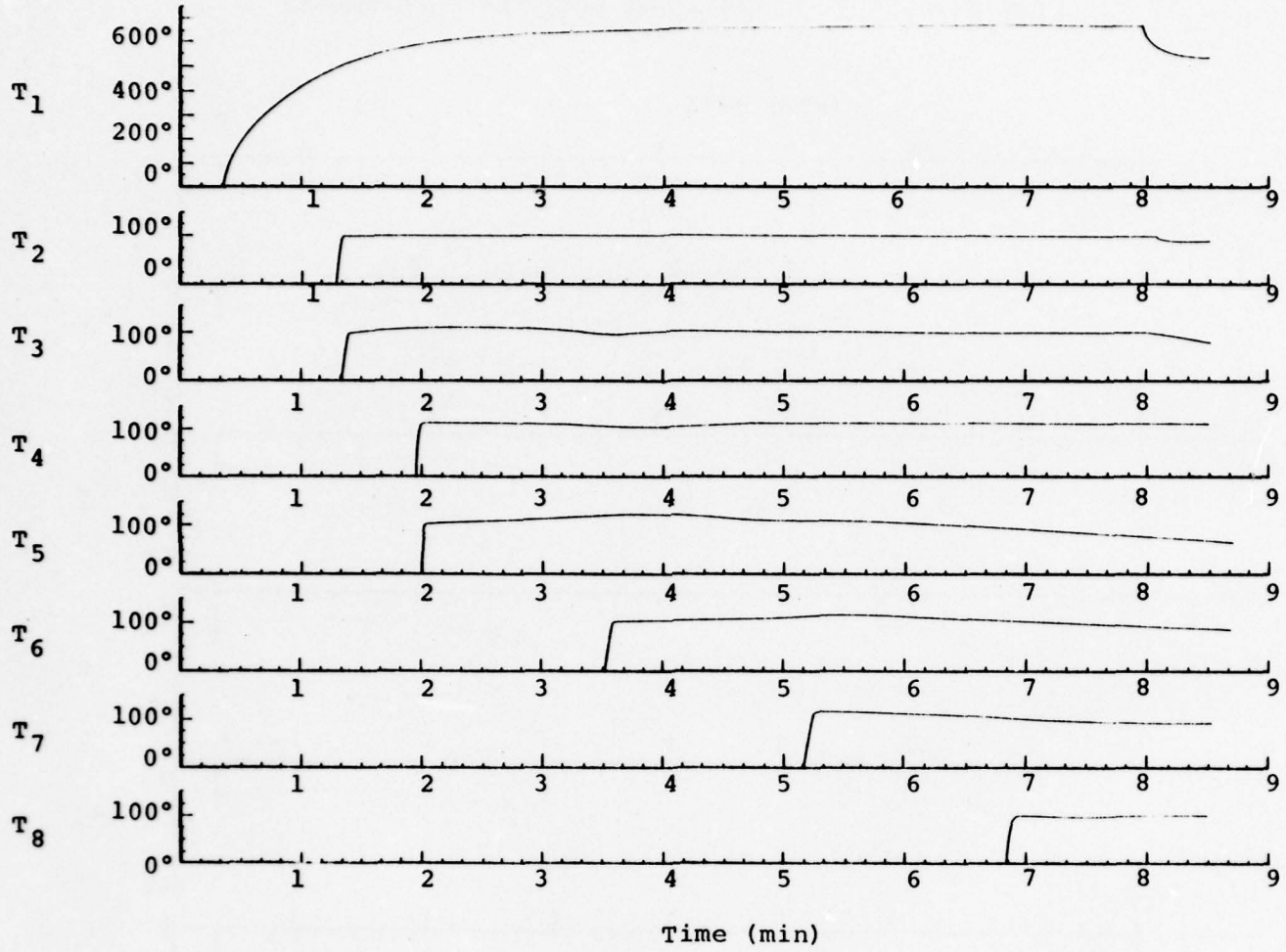

Temperature Versus Time for Experiment of 4/19/78.

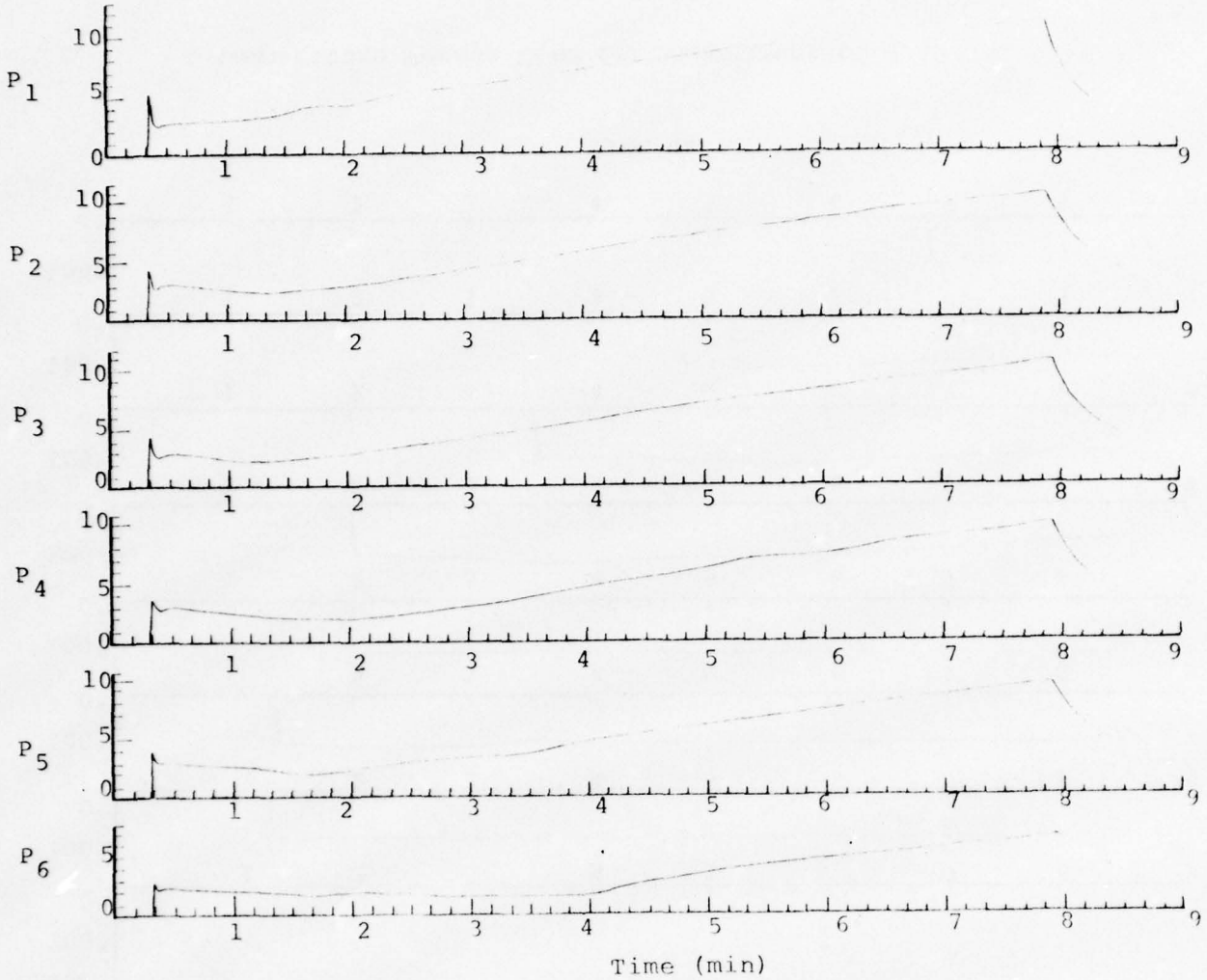

Pressure Versus Time for Experiment of 4/19/78.

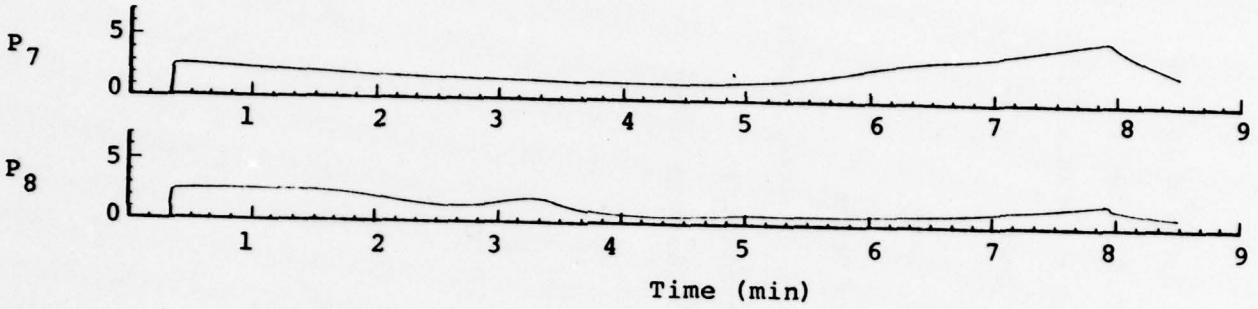

Pressure Versus Time for Experiment of 4/19/78.

EXPERIMENT VII (4/20/78)

Total Mass of Sand = 1.679×10^5 gm

Moisture (initial) = .05% (Dry)

Available Volume Sand = 1.038×10^5 cc

$\rho_{bulk} = 1.618$ gm/cc

$\phi = 39\%$

$S = 0.2\%$

Flow Input = 6 gm/sec Steam

Initial Permeability = 25 darcy (measured)

T_1 is "K" Thermocouple

T_2-T_8 are "J" Thermocouples

EXPERIMENT VII (4/20/78)

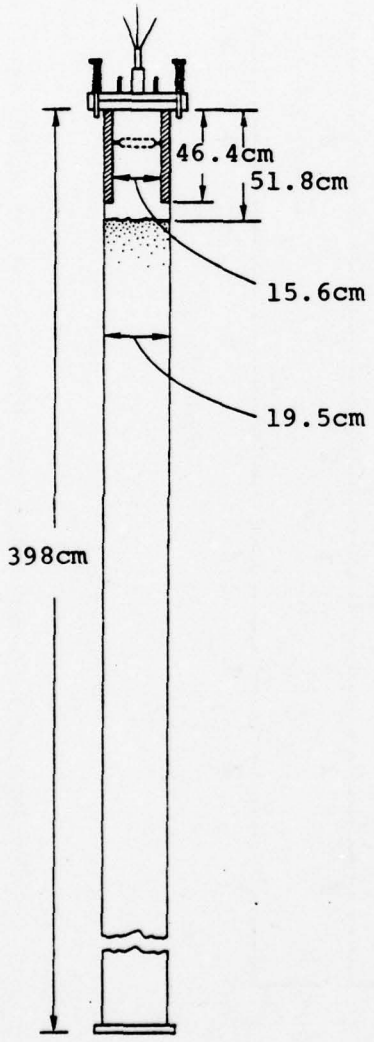

T_1 is torch diagnostic

Location (Below Sand)

T_2	5.6cm	1.25cm off center
T_3	12.6cm	1.25cm off center
T_4	12.6cm	5.0 cm off center
T_5	31.4cm	1.25cm off center
T_6	72.0cm	1.25cm off center
T_7	121.0cm	1.25cm off center
T_8	154.4cm	1.25cm off center

P_1 is torch diagnostic

P_2	5.4cm	1.25cm off center
P_3	12.6cm	1.25cm off center
P_4	12.9cm	5.0 cm off center
P_5	32.0cm	1.25cm off center
P_6	72.1cm	1.25cm off center
P_7	120.7cm	1.25cm off center
P_8	154.6cm	1.25cm off center

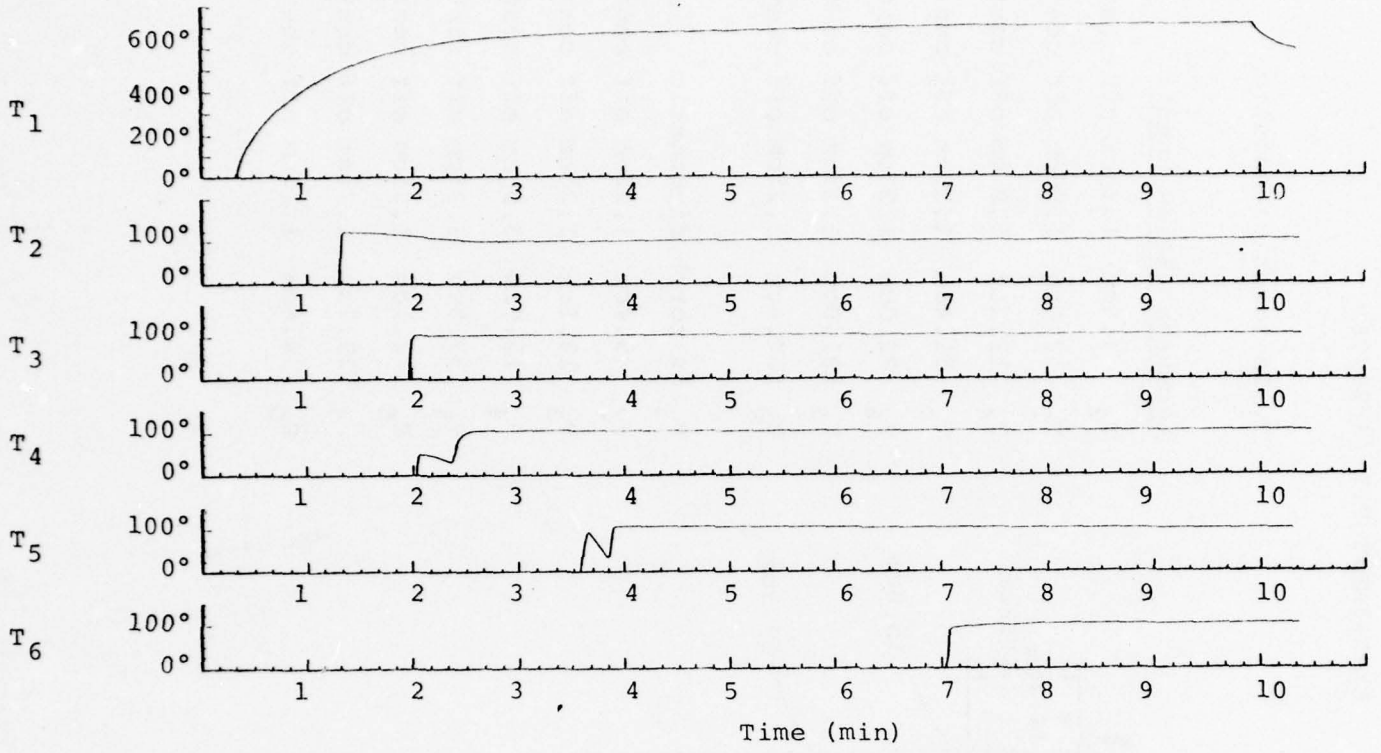

Temperature Versus Time for Experiment of 4/20/78.

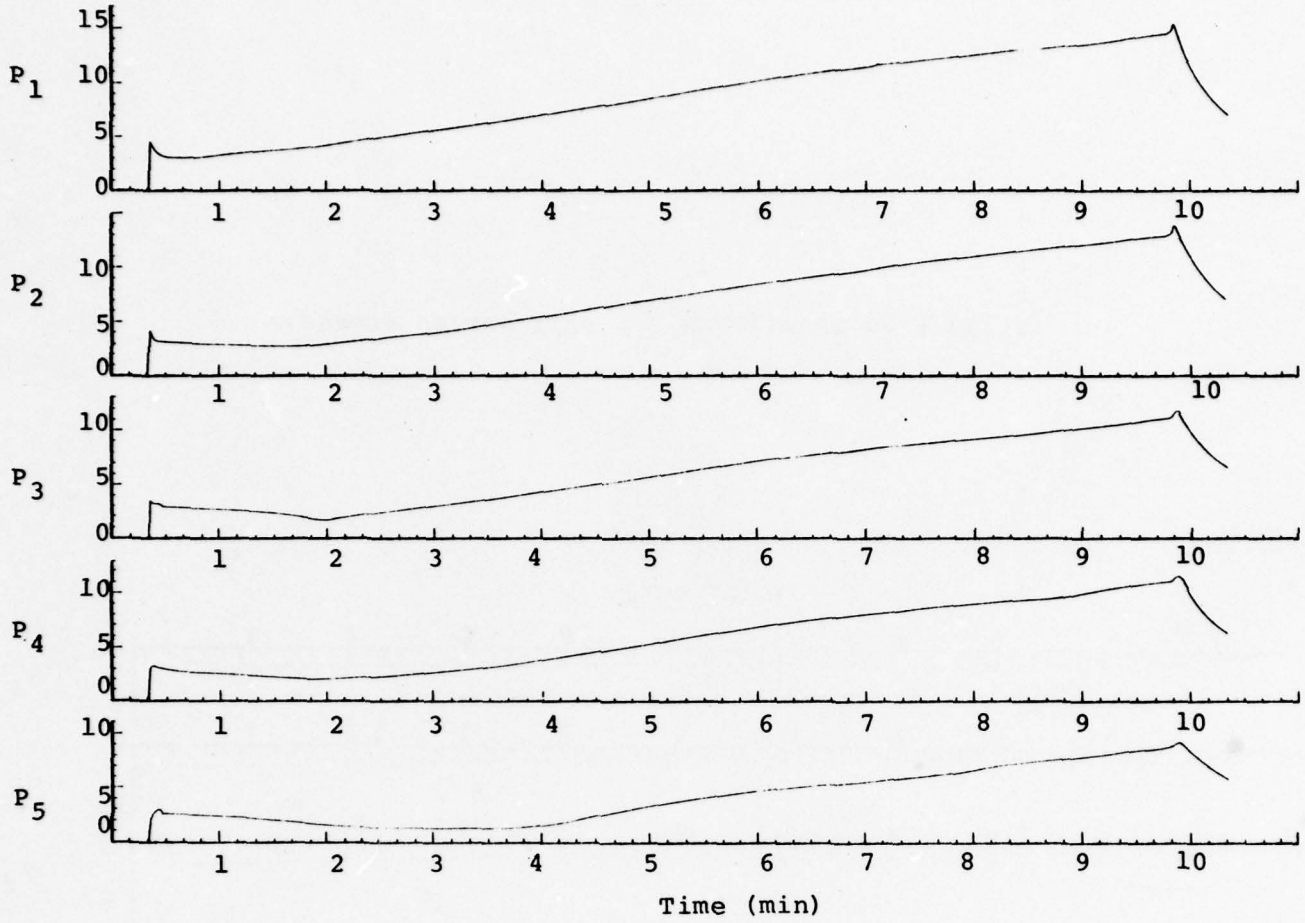

Pressure Versus Time for Experiment of 4/20/78.

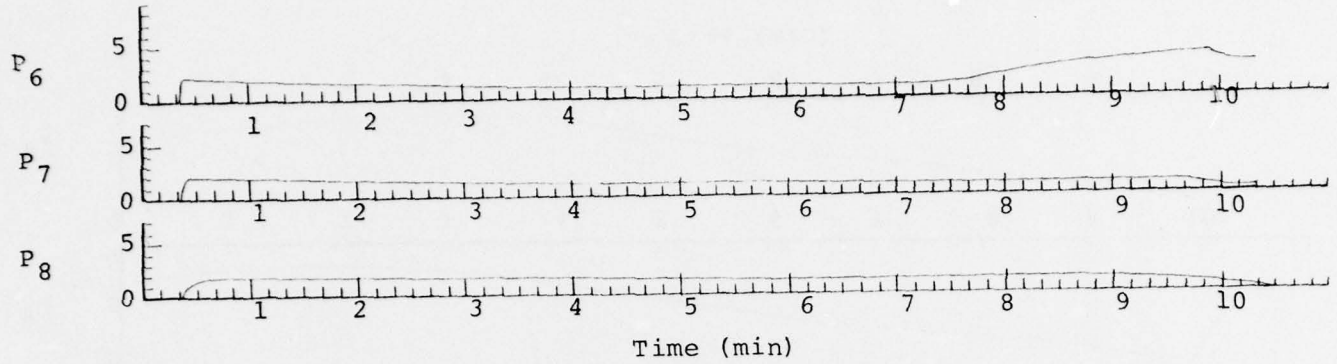

Pressure Versus Time for Experiment of 4/20/78.

EXPERIMENT VIII (4/21/78)

Total Mass of Sand = 1.707×10^5 gm

Moisture (initial) = 0.08% (Dry)

Available Volume for Sand = 1.037×10^5cc

ρ_{bulk} = 1.646 gm/cc

ϕ = 38%

S = 0.3%

Flow Input = 6 gm/sec Steam

Initial Permeability = 24 darcy (measured)

T_1 is "K" Thermocouple

T_2-T_8 are "J" Thermocouples

EXPERIMENT VIII (4/21/78)

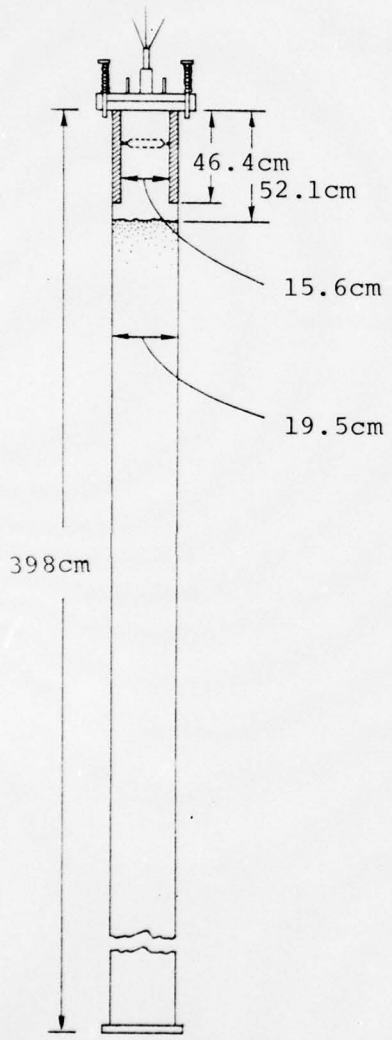

Transite Pipe

T_1 is torch diagnostic

Location (Below Top of Pipe)

T_2	5.3cm	1.25cm off center
T_3	12.3cm	1.25cm off center
T_4	12.3cm	5.0 cm off center
T_5	31.1cm	1.25cm off center
T_6	71.7cm	1.25cm off center
T_7	94.7cm	1.25cm off center
T_8	120.7cm	1.25cm off center

P_1 is torch diagnostic

P_2	5.1cm	1.25cm off center
P_3	12.3cm	1.25cm off center
P_4	12.6cm	5.0 cm off center
P_5	31.7cm	1.25cm off center
P_6	71.8cm	1.25cm off center
P_7	94.5cm	1.25cm off center

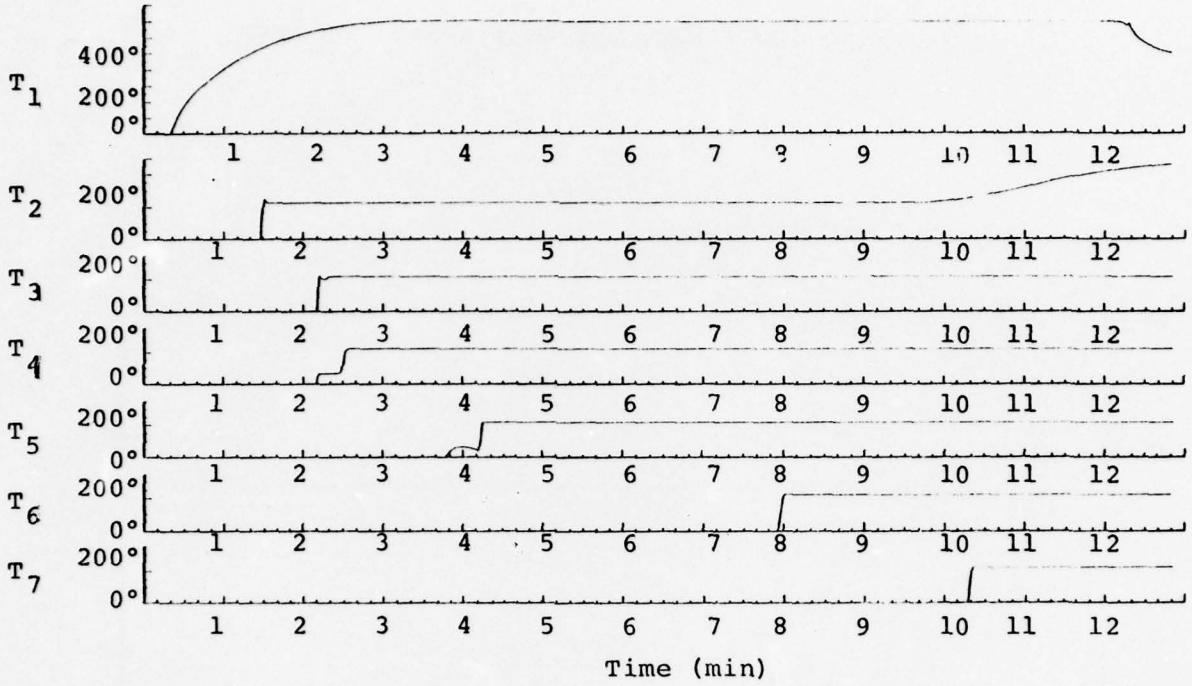

Temperature Versus Time for Experiment of 4/21/78.

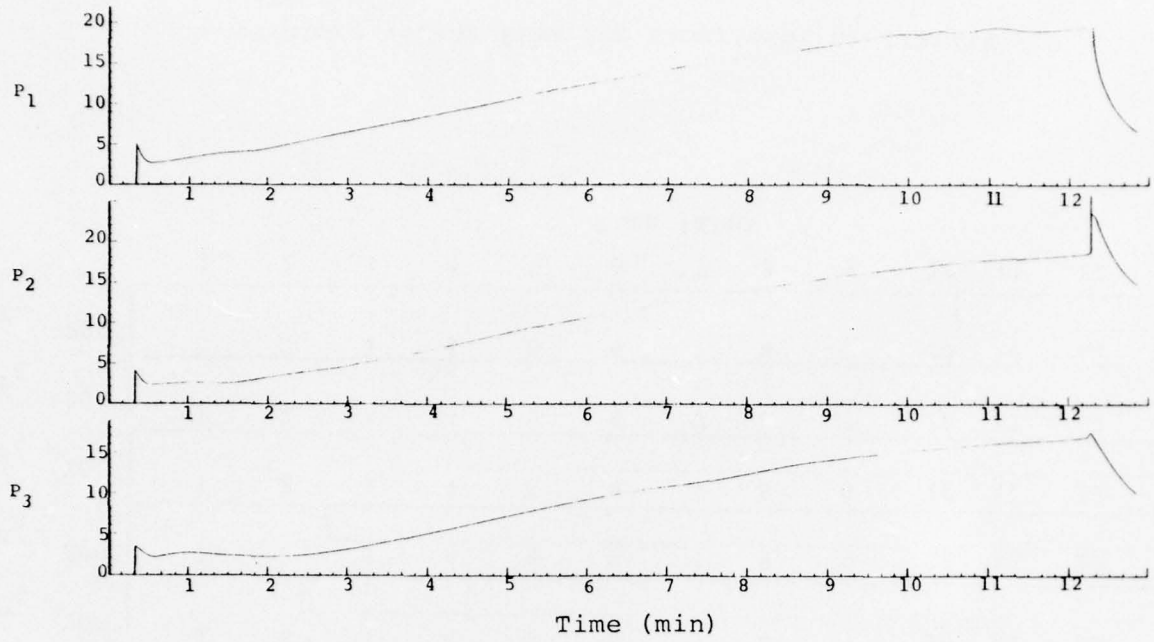

Pressure Versus Time for Experiment of 4/21/78.

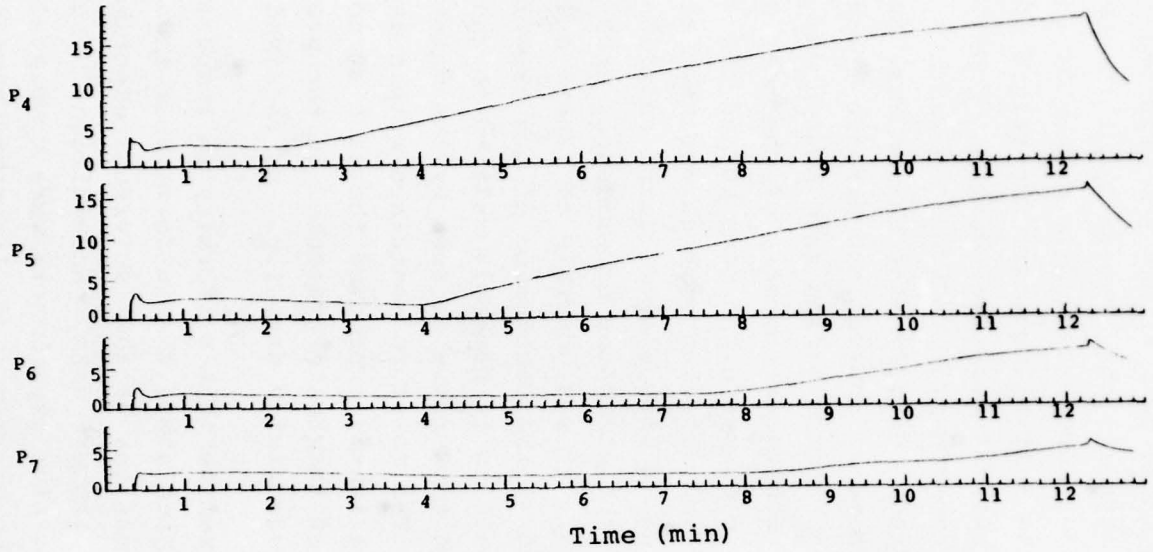

Pressure Versus Time for Experiment of 4/21/78.

V. DISCUSSION

In this section we shall briefly discuss each of the successful experiments whose data traces are provided in the previous chapter. One general observation about the experiments performed is that it was exceedingly difficult to obtain consistent data when the initial moisture was raised above the "as received" 0.1 percent moisture content. Experiments II and V are the only experiments provided for which a higher moisture content was used. Usually what happed was, during the course of the experiment, unusual and erratic traces were recorded; in some cases, thermocouples were burned out during the recording period. Subsequent reentry of the test chamber showed that thermocouple elements had been burned off at the sensing head. In addition, the sand, which was initially emplaced well-packed, had a flocculated "fairy castle" structure to it. In one of the attempted experiments, (not listed in the previous section), it was possible to insert a 1 cm rod 90 cm into the sand at the conclusion of the experiment. This flocculating or bulking is probably related to the fact that the steam at these flow rates is seen by the moist sand as extremely hot air. The moisture contained within the sand is rapidly dried out, slightly expanding the sand structure. For this reason, most of the tests presented in the previous section were done on essentially dry, i.e., as received sand.

Based on the premise that uniformity in temperature arrivals implies something about the uniformity of the steam front most of the discussions of the individual experiments will center on the temperature data. An additional detail is that after the first five experiments were completed, it became apparent that the ceramic fiber liner may have been causing a problem in the measurements. The liner is axially permeable and apparently allows steam flow down the side of

the pipe into the sand. The actual thermal front due to steam arriving at the sand surface arrived later at the thermocouple positions.

Experiment I shows reasonable planarity of the steam front as evidenced by the approximate simultaneity of arrivals at thermocouples T-2, T-3, and T-4, and similar simultaneity at thermocouples T-5, T-6, and T-7. We notice, however, at somewhat later times especially at thermocouple T-3, evidence of inhomogeneities beginning within the flow. The temperature at that station begins to rise rather markedly around 2.5 to 3.0 minutes into the test.

The pressure traces shown in Experiment I all exhibit the characteristic pressure spike at the initiation of the experiment. This spike is due to the ignition of hydrogen and oxygen at zero time. The experimental procedure used was to allow hydrogen/oxygen to flow into the test chamber for three seconds prior to turning on both the water flow and igniting the sparker system. Positive evidence of ignition of the hydrogen/oxygen mixture is shown by these pressure pulses.

Experiment II is performed with moisture content of 3.3 percent. The nominal flow input of steam is identical from Experiment I to Experiment II, yet the pressure trace records rather graphically the fact that steam flow was retarded in the sand column during this experiment. Note also that at thermocouple locations T-2, T-3, and T-4, there is evidence of nonhomogeneity of temperature arrival. The steam front seems to be fairly planar by the time of arrival at thermocouple locations 5, 6, and 7. Further evidence of problems with the flow are evident by examining thermocouple trace T-3 where temperature begins to rise rather drastically at four minutes and twelve seconds into the test.

Experiment III was performed on essentially dry sand. The pressure traces, especially P-1, contained an inordinate amount of noise. These spikes evident on trace P-1 are electrical in nature and are artifacts of problems in the recording system. We do not believe they were occurring in the steam production within the test volume. This particular test seems to be plagued with problems at early times, as can be seen by looking at relative arrival times of T-2, T-3, and T-4. Also note that temperatures begin to rise drastically on thermocouple T-3 at one minute and fifty seconds into the test. Reasonable homogeneity seems to be in evidence for the remainder of the test, as can be seen by inspecting thermocouples T-5, T-6, T-7, and T-9. T-9 was located on the outside wall just slightly into the sand at the same nominal depth of burial as T-5, 6, and 7. Arrival times are consistent.

Experiment IV demonstrates the degree of planarity of the steam front. Thermocouple locations T-2, T-3, and T-4 do not agree as well as might be guessed from studying the traces, since T-3 is (1.0 centimeter) deeper than T-2 and 1.3 centimeters deeper than T-4. Arrival at locations T-5, T-6, T-7, and T-9 are similar to those in Experiment III. They indicate a nonhomogeneity in the temperature front seen in this experiment.

Experiment V was also performed with a nonzero initial moisture content. The pressure traces are seen to be intermediate between the traces exhibited in, say Experiment I where the sand was essentially dry, and Experiment II where the sand was more saturated than any other test. Scatter is apparent in the temperature arrivals. Locations T-3, T-4, T-5, and T-6 show reasonable agreement in arrival times. No recordings were obtained from Location T-2 or T-7 for this particular run. This was probably the better of the two data sets taken for the non-dry sand column.

Experiments VI, VII, and VIII were performed some six months later after it became apparent that the ceramic fiber liner protruding into the sand layer may be causing a problem. These experiments were all performed on nominally dry (as received) sand. The sand, however, was from a different lot from the sand used in the initial five experiment. Comparing the measured permeabilities, it is somewhat different from the initial lot. These experiments, we feel are much more believable than the previous five.

The precursors seen on T-4 and T-5 in Experiment VII are artifacts of the thermocouple, i.e., we believe there was a break in the thermocouple which was healed by the increased temperature. The time of arrival for the thermal wave at this location should be taken as the initial rise in the thermocouple. This same observation holds true for T-4 and T-5 in Experiment VIII. Note that at very late times in Experiment VIII (ten minutes into the experiment) temperatures begin to rise rather dramatically at T-2. This suggests either that the sand was being blown away from the thermocouple by this time or that the temperature in the steam was beginning to rise as the pressure increased. For purposes of comparison with calculations, the data obtained in Experiments VI, VII, and VIII should take priority over Experiments I through V since the flow through the cylindrical liner must be taken into account in order to appropriately model the steam flow and subsequent temperature arrivals within the pipe for these first five.

A point which should be emphasized is that most of the experimental problems which were encountered during this year's experimental effort had to do with obtaining data within a packed steam pipe. In general they had nothing to do with the performance of the steam generating torch. In fact, in well over the sixteen times the torch was actually

used in an experiment, there was no indication of torch failure, save for one faulty ignition sequence during which time a test was started and the spark gap failed. The primary purpose of the development effort was to demonstrate the experimental feasibility of a hydrogen-oxygen-water steam generating system. We believe that we have adequately demonstrated both the controllability and safety of such a system. We feel that a scaled-up version of this generator would be ideal for generating steam-driven hydrofracs in a variety of geologically interesting media.

In addition, it is conceivable that such a steam generating source may find additional applications in the areas of tertiary oil recovery, oil shale retorting, and in any region in which copious quantities of steam are required and in which it is not desired to go to the expense and trouble of constructing a full-scale steam generating plant.

REFERENCES

Lewis, Bernard; and Von Elbe, Gunther: Combustion, Flame and Explosion of Gases. Second ed., Academic Press, 1961.

Drell, Isadore L.; and Belles, Frank E.: Survey of Hydrogen Combustion Properties. NASA Rept. 1383, Lewis Flight Propulsion Laboratory, Cleveland, Ohio, 1958.

Grumer, J.; Strasser, A.; and Van Meter, R. A.: Principles for Safe Handling of Liquid Hydrogen. Tech. Report SNC-21, Bureau of Mines, Pittsburgh, PA, 1967.

Chelton, D. V.: Safety in the Use of Liquid Hydrogen. Technology and Uses of Liquid Hydrogen, MacMillan Co., 1964, pp. 359-378.

Weintraub, A. A.: Control of Liquid Hydrogen Hazards at Experimental Facilities: A Review. Report HASL-160, Health and Safety Laboratory, New York Operations Office, AEC, 1965.

Caras, G. J.: Prevention, Detection, and Suppression of Hydrogen Explosion in Aerospace Vehicles. RSIC-486, Redstone Arsenal, Ala., 1966.

Coward, H. F.: and Jones, G. W.: Limits of Flammability of Gases and Vapors. Bull. 503, U. S. Dept. of the Interior, Bureau of Mines, Washington, D. C., 1952.

Profitt, R. L., et al.: Saturn Fire Detection Systems R-6616. Rocketdyne Division, North American Rockwell Corp., Canoga Park, CA, 1967.

Cassutt, L. H.; Maddocks, F. E.; and Sawyer, W. A.: A Study of the Hazards in the Storage and Handling of Liquid Hydrogen. Advances in Cryogenic Engineering, Vol. 5, Plenum Press, Inc., 1960.

Zabetakis, M. G.; Furno, A. L.; and Perlee, H. E.: Hazards in Using Liquid Hydrogen in Bubble Chambers. Report of Investigations 6309, U. S. Department of the Interior, Bureau of Mines, Washington, D. C., 1963.

Anon.: Report on Investigation of Explosion and Fire. Experimental Hall, CEA, Report TID-22594, U. S. AEC, 1966.

Gaydon, A. G.; and Wolfhard, H. G.: Flames, Their Structure, Radiation and Temperature, 2nd. Ed., Chapman and Hall, (London), 1960.

Rosen, B.; Dayan, V. H.; and Proffit, R. C.: Hydrogen Leak and Fire Detection. NASA Publication SP-5092, U. S. Government Printing Office, Washington, D. C., 1970.

APPENDIX A1
CYLINDRICAL CAPACITOR SATURATION GAUGE

In this appendix we discuss the theory of a cylindrical capacitor used as a saturation gauge. In addition, we present the data recorded from two successful experiments in which saturation was measured. Given two coaxial cylinders of radii a and b with length ℓ, which are given equal and opposite charges, +q and -q; we create a cylindrical capacitor (see Figure A1-1). We now take as a Gaussian surface a cylinder of radius r intermediate between a and b and of length ℓ (neglecting end effects). Lines of displacement cut this surface only over the curved surface of area $2\pi r\ell$. If we let D represent the displacement vector of radius r, then

$$\int \overline{D} \cdot d\overline{A} = 2\pi r\ell D = q \qquad \text{(A1-1)}$$

$$D = \frac{q}{2\pi r\ell} \quad . \qquad \text{(A1-2)}$$

If the material between the cylinders contains a dielectric of permitivity ε, the electric field E is

$$E = \frac{D}{\varepsilon} = \frac{1}{2\pi\varepsilon}\frac{q}{r\ell} \quad . \qquad \text{(A1-3)}$$

The magnitude of the potential difference between the cylinders is

$$V_{ab} = \int_a^b E dr = \frac{1}{2\pi\varepsilon}\frac{q}{\ell}\int_a^b \frac{dr}{r} \qquad \text{(A1-4)}$$

$$= \frac{1}{2\pi\varepsilon}\frac{q}{\ell}\ell n\frac{b}{a} \quad .$$

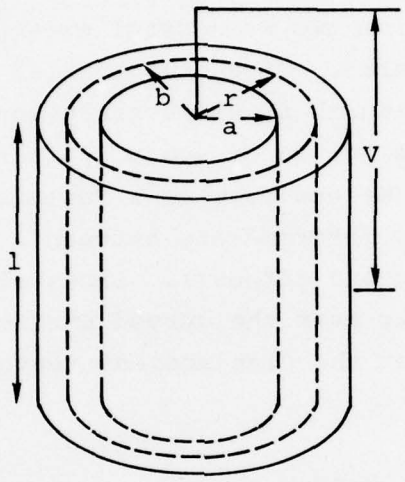

FIGURE A1-1. CYLINDRICAL CAPACITOR

The capacitance is, therefore,

$$C = \frac{q}{V_{ab}} = 2\pi\varepsilon \frac{\ell}{\ell n\ b/a} \qquad \text{(A1-5)}$$

During the course of these experiments we measured the capacitance of the cylindrical capacitor using a Hewlett-Packard reactance meter.

This device allows us to measure capacitances as low as 1 picofarad. Given the relation A1-5, we may then generalize the equation to a case where materials possessing different permitivity are mixed.

If ε = total permitivity, then

$$\varepsilon = [(1-\phi)\ \varepsilon_{sand} + \phi S\ \varepsilon_{H_2O}] \qquad \text{(A1-6)}$$

where ε_{sand} = permitivity of dry sand

ε_{H_2O} = permitivity of water

S = saturation percentage

ϕ = porosity

Generalizing equation (A1-5)

$$C = \frac{2\pi\ell}{\ell n\ b/a} [(1-\phi)\ \varepsilon_{sand} + \phi S\ \varepsilon_{H_2O}] \qquad \text{(A1-7)}$$

We can use relation A1-7 to infer an expected change in capacitance due to change S by taking differentials.

$$\Delta C = \frac{2\pi\ell}{\ell n\ b/a} \Delta S \phi \varepsilon_{H_2O} \qquad \text{(A1-8)}$$

Then,

$$\frac{\Delta C}{C} = \frac{\phi \varepsilon_{H_2O} \Delta S}{(1-\phi)\varepsilon_s + \phi S \varepsilon_{H_2O}} \qquad \text{(A1-9)}$$

$$= \frac{\phi \Delta S}{(1-\phi)\frac{\varepsilon s}{\varepsilon_{H_2O}} + \phi S}$$

Since,

$$\varepsilon_{sand} = 4.3$$

and,

$$\varepsilon_{H_2O} = 78.5$$

$$\frac{\Delta C}{C} = \frac{\phi \Delta S}{0.055(1-\phi) + \phi S} \qquad \text{(A1-10)}$$

From this relation the change in capacitance can be related to the change in saturation of the cylindrical capacitor.

In Figure A1-2 we present a plot of equation A1-10. Note that in the saturation intervals of interest there appears to be substantial capacitance change.

Since it is difficult to exactly reproduce moisture conditions with a capacitor packed with sand, we have to settle for checking relation A1-10 against some easily measurable limits. These are presented in Table A1-1.

Reasonable agreement is apparent. The measured value is always higher than the calculated value suggesting that edge effects are important.

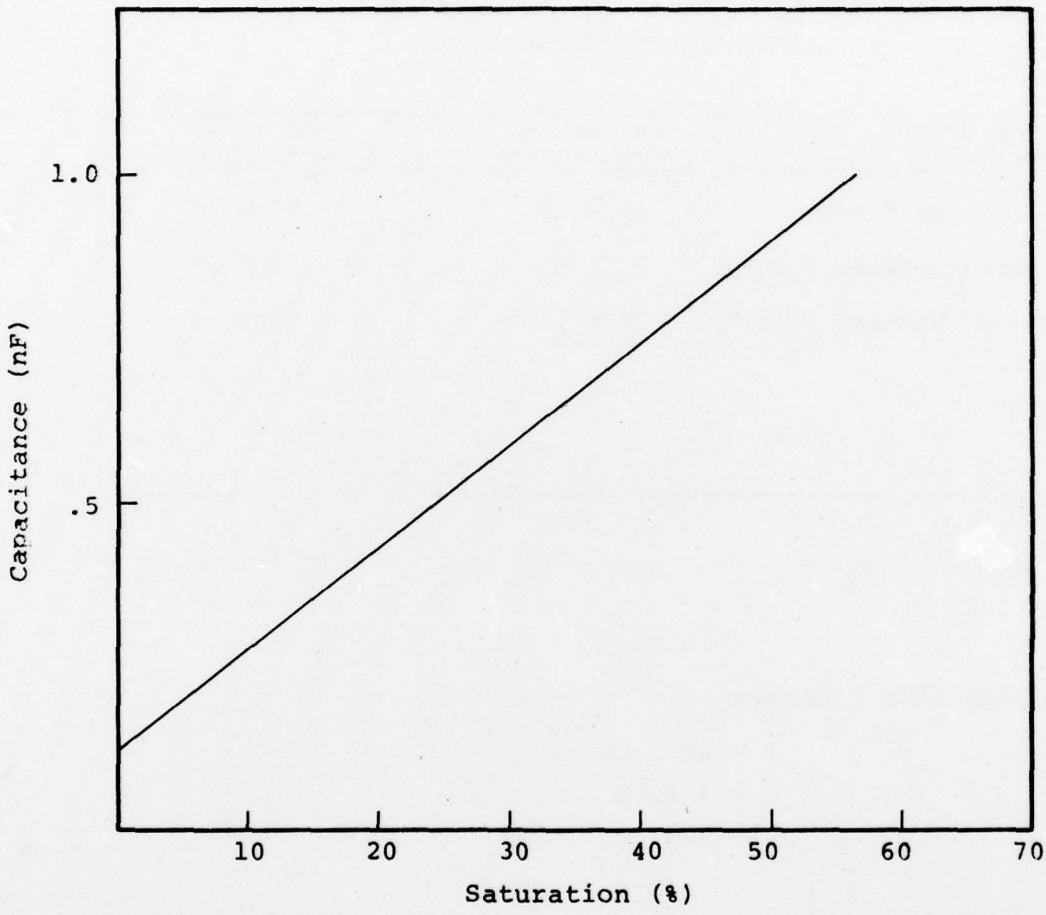

Figure A1-2. Theoretical Change of Capacitance with Saturation.

TABLE A1-1

CALCULATED AND MEASURED CAPACITANCE FOR

CYLINDRICAL CAPACITOR

Experiment Condition	Calculated Capacitance	Measured Capacitance
Air Between Plates	49.3 pF	57.4 pF
Dry Sand Between Plates	127 pF	167 pF
Pure H_2O Between Plates	3870 pF	5440 pF

Capacitor Dimensions:

ℓ = 10.2 cm

a = 4.1 cm

b = 5.5 cm

Actual data from two experiments are presented in Figure A1-3 and A1-4. In Figure A1-3, the top of the capacitor was 18.1 cm below the sand level and was centered on the axis of the pipe. In Figure A1-4, the top of the capacitor was located 25.6 cm below the sand surface.

Using relation A1-10 and the values initially measured for moisture within the sand, it is possible to infer a change in saturation from the measured change in capacitance. For the test of 8/11/77, $\Delta S = 0.06$ while for 8/30/77 the change was 0.04. In the test of 8/11/77 the capacitor was uncovered immediately after ending the test. A determination of moisture in the sand on the axis of the capacitor gave $w = 1.5\%$. This implies a saturation of 0.06 which is the same as calculated.

This agreement may be fortuitous since only one such confirming test was made. The agreement does suggest that the change in capacitance can be related to saturation percentage extant in the sand columns.

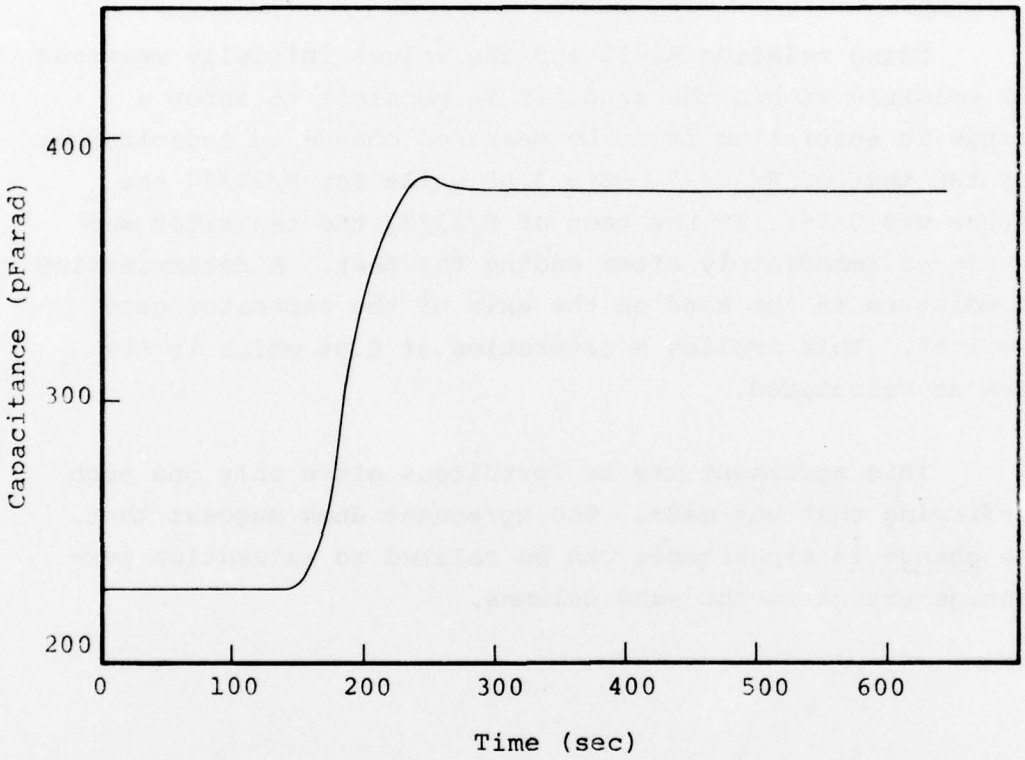

Figure A1-3. Capacitance Versus Time from Test of August 11, 1977.

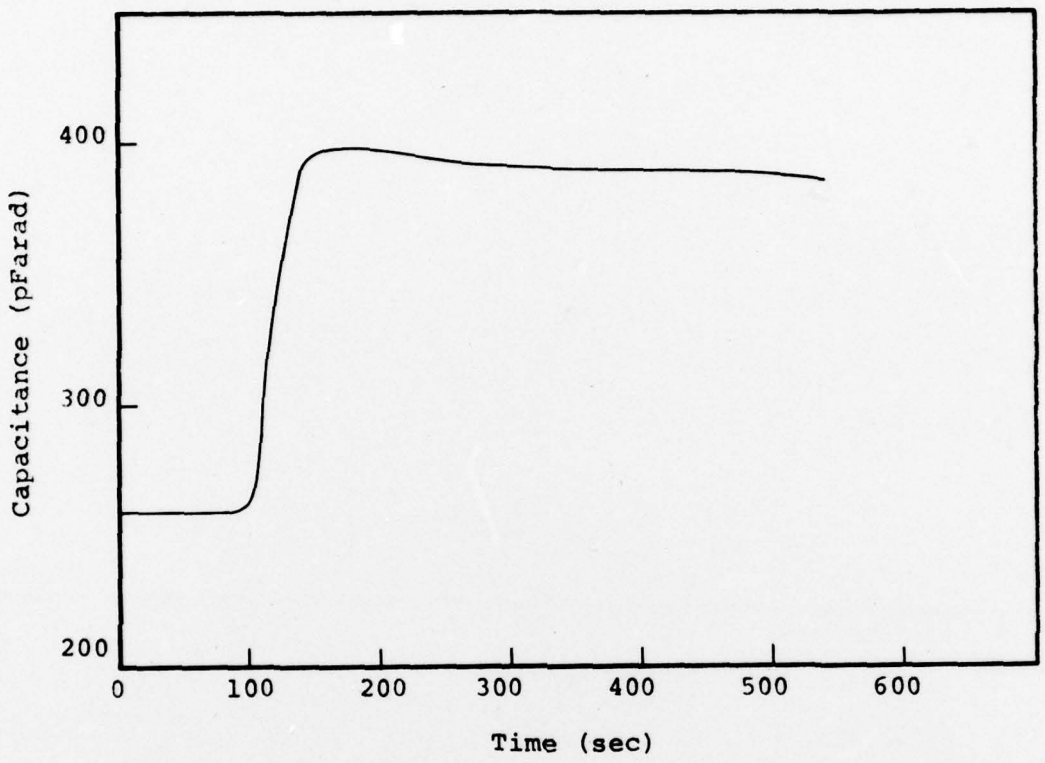

Figure A1-4. Capacitance Versus Time from Test of August 30, 1977.

APPENDIX A2

Given a pipe of length L, containing a substance of porosity ϕ, we are interested in determining the mean permeability exhibited by the material in the pipe. Injecting gas with a known pressure and flow rate under steady state conditions. It is known that under these conditions the flow rate of gas into such a pipe is given by the following equation:

$$\dot{W} = A \frac{\rho_0}{\frac{1}{\rho^{\gamma}}} \frac{K}{L\mu} \frac{\gamma}{\gamma+1} \left[P_0^{\frac{\gamma+1}{\gamma}} - P_{Atmosph}^{\frac{\gamma+1}{\gamma}} \right] \qquad \text{(A2-1)}$$

where

$\dot{W}$ = mass flow rate
A = pipe area
L = pipe length
P_0 = driving pressure
$P_{atmosph}$ = atmospheric pressure
ρ_0 = gas density at driving pressure
K = permeability
μ = gas viscosity
γ = compressive index

For the purpose of this particular experiment, we can assume isothermal conditions, i.e., $\gamma = 1$, then for the following parameters which are characteristics of the experiment undertaken to determine flow characteristics:

$P_0 = 5$ psig $= 1.34$ atmosphere
$\rho_{atmosph} = 0.00129$ gm/cc
$A = 298.6$ cm^2
$\mu = 1.8 \times 10^{-4} \frac{\text{dyne sec}}{\text{cm}^2}$

We obtain a relation for permeability

$$K = \text{flow} \times L \times 0.0012 \qquad \text{(A2-2)}$$

where

K is in darcies
L is in cm
and flow is in standard cubic feet per hour.

By setting the driving pressure at 5 psig and monitoring the flow rate, eq. (A2-2) was utilized to infer initial permeabilities in the pipe.

In total, eight distinct permeability measurements were performed for eight of the nineteen experiments undertaken. For completeness, we present in Table A2-1, the results of these sets of measurements taken in pipes having different moisture contents and different initial starting densities. Aside from the test on 8/30/77, the bare pipe leak was less than 0.1 scfh. The measured value of the leak recorded for the measurement on 8/30/77 was 5 standard cubic feet per hour at a driving pressure of 5 psig. The experiments of 8/30/77 and 11/4/77 were taken with sand in approximately the same moisture condition. We believe this indicates the degree of reproducibility of the combination of the measurement and our sand packing capability. The measurements of 8/30/77 had a net corrected input flow of 95 scfh, while the measurements on 11/4/77 had an input flow of 90 scfh. This difference implies a 6 percent variation in the inferred permeability. Such variation, we feel, is considerably smaller than the uncertainties inherent in the rest of these measurements.

The inferred permeabilities in the experiments of 4/19, 4/20 and 4/21 are significantly lower than for the other tests. These tests were run with sand from a different lot ordered at a later time from the first batch. Differences between lots probably account for the difference in permeabilities.

TABLE A2-1

FLOW DATA IN SAND FILLED PIPE

Experiment	P_0 (psig)	ρ_{bulk} (gm/cc)	w(%)	L(cm)	Flow (SCFH)	K (Darcy)
8/30/77	5	1.646	0.1	369	95	42
11/1/77	5	1.374	2.5	373	172	77
11/2/77	5	1.433	2.2	375	162	72
11/3/77	5	1.438	4.0	374	145	65
11/4/77	5	1.415	0.1	376	90	41
4/19/78	5	1.590	0.05	347	60	25
4/20/78	5	1.618	0.2	347	60	25
4/21/78	5	1.646	0.08	347	57	24

TABLE A3-1

PHYSICAL PROPERTIES OF CERAMIC FIBER LINERS[†]

	Engineering Units	SI
Density	35 lbs/ft^3	0.56 gm/cc
Thermal Conductivity	0.8 BTU inch/hr ft^3°F at 1000°F	0.14 joule/ hrcm^2°C
Specific Heat	0.27 BTU/lb°F	1.13 joule/gm°C

[†]Data courtesy of Aerospex Corporation, a registered distributor of Carborundum Corporation.

APPENDIX A3

PHYSICAL PROPERTIES OF CERAMIC FIBER LINER

The ceramic fiber liner and blast deflector are made from layers of woven silica/alumina manufactured by the Carborundum Corporation. The layers are shaped in a dry state, thoroughly soaked with a rigidizing agent and then fired in an oven at 600°F overnight.

Representative physical properties are presented in Table A3-1. In addition, radial and axial flow tests were undertaken to provide data with which to infer permeability. A photo of the experimental set-up is presented in Figure A3-1.

In the radial flow experiment, axial flow was precluded by use of poured epoxy and plugs. These plugs covered the top and bottom of the ceramic fiber cylinder and allowed flow only in the radial direction.

For the axial flow test, a solid cylinder was bonded inside the ceramic fiber cylinder. The outer surface of the ceramic fiber cylinder was coated with epoxy. A grooved plate was cemented to the bottom annular surface of the liner. This was further secured by means of large "C" clamps. This plate served to pressurize one annular face of the liner. Pressures were monitored with a Validyne Model DP-15 differential pressure transducer. Flows were measured with a Dwyer 5-50 SCFH rotometer.

Radial permeabilities were calculated utilizing the relation:

$$K = 8.99 \frac{\mu}{L} \frac{P_\infty}{\rho_\infty} \frac{\ln r_0/r_\infty}{P_0^2 - P_\infty^2} \dot{W}$$

Figure A3-1. Flow Test Apparatus for Flow Tests on Ceramic Fiber Liner. Test Block for Axial Test is in Center of Photo. Test Fixture for Radial Test is on the Left. A Validyne Transducer Readout is in front of a Flow Monitoring Panel on the Left.

where $\dot{W}$ = mass flow rate

μ = gas viscosity

L = cylinder length

P_∞ = reference pressure (atmosphere)

ρ_∞ = reference density of gas (atmospheric pressure)

r_∞ = inner radius

P_0 = driving pressure

r_∞ = outer radius

Axial permeability was inferred using the equation:

$$K = \frac{\mu L}{Q^* \rho_0 A} \frac{P_0 \dot{W}}{P_0^2 - P_\infty^2}$$

where μ, P_0, P_∞, and $\dot{W}$ are as defined above

ρ_0 = gas density at driving pressure

A = area across which gas flows

Q^* = conversion factor to Darcy (9.87×10^{-9})

TABLE A3-2

AXIAL PERMEABILITY

$L = 15cm$
$A = 109cm^2$

Pressure (psig)	Flow Rate (SCFH)†	K (Darcy)
1	17	0.162
2	28	0.134
3	35	0.108
4	43	0.095
5	49	0.082

†Steady state flow

AD-A074 371 SYSTEMS SCIENCE AND SOFTWARE LA JOLLA CA F/G 18/3
HYDROGEN, OXYGEN, WATER STEAM GENERATOR.(U)
OCT 78 P LAGUS
UNCLASSIFIED SSS-R-79-3813 DNA001-77-C-0188 DNA-4733F NL

2 OF 2
AD
A074371

END
DATE FILMED
10-79
DDC

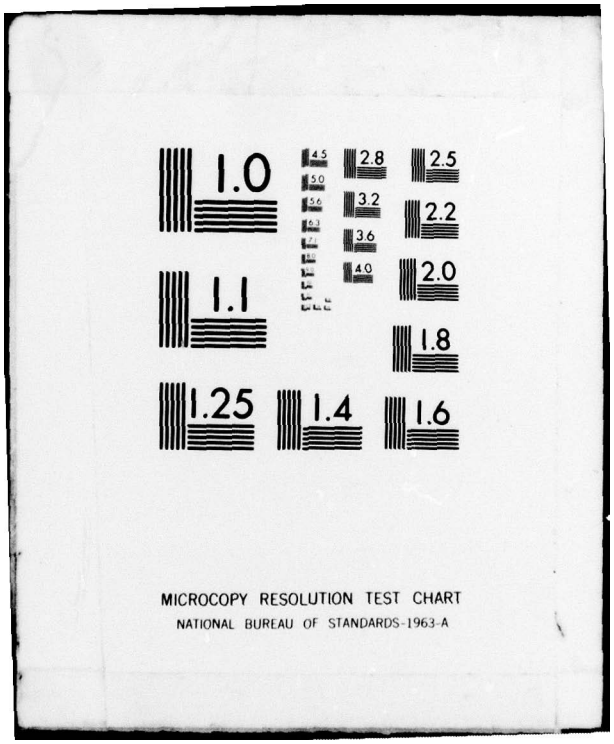
1.0
1.1
1.25
1.4
1.6
1.8
2.0
2.2
2.5
2.8
3.2
3.6
4.0
4.5
5.0
5.6
MICROCOPY RESOLUTION TEST CHART
NATIONAL BUREAU OF STANDARDS-1963-A

TABLE A3-3

RADIAL PERMEABILITY

L = 5.6cm

r_0 = 3.06cm

r_∞ = 3.84cm

Pressure (psig)	Flow Rate (SCFH)†	K (Darcy)
1	14	0.16
2	24	0.13
3	30	0.11
4	36	0.10
5	40	0.08

†Steady state flow

APPENDIX A4

Undoubtedly, hydrogen is a hazardous material. It is readily flammable in air and creates explosive mixtures with air. Because its flammability limits when mixed with air are very wide and its ignition energy is very small, a hydrogen fire is easier to create than a methane or gasoline fire. The required safety precautions for handling hydrogen are, therefore, more stringent than those required for conventional gases or fuels.

HYDROGEN COMBUSTION PROPERTIES

The principal reason for considering hydrogen a hazardous material is its flammability and detonability in air over a wide range of conditions. Hydrogen combustion has been the subject of much study. Lewis and Von Elbe's basic text (ref. 1) presents a summary of combustion phenomena, including some data on hydrogen combustion. References 1 and 2 are valuable compilations which concentrate on hydrogen combustion properties. References 3, 4 and 5 contain summaries of properties relating to the combustion hazards of hydrogen in air.

A mixture of hydrogen and air may be ignited in several ways, and the resulting flame may propagate in various ways. The conditions affecting the ignition characteristics include: contents of the gas mixture, temperature, pressure, geometry of the surrounding walls, ignition energy and, in some cases, gas velocity. Such conditions determine whether there will be no ignition, a stationary flame at a source of hydrogen gas, a deflagration through a volume of gas, or a detonation. Ignition sources may be a hot solid body, a flame or other hot gas, an explosive charge, or an electric spark.

Combustion can propagate through a hydrogen air mixture either as a deflagration, a deflagration which grows to a

detonation, or as a detonation from the start of ignition. In a confined space, a deflagration can raise the pressure by about a factor of 7- enough to cause some structural damage. A detonation can cause a very rapid rise in pressure by as much as 20 times the initial pressure (ref. 3). Either of these processes may be accompanied by a sound (sometimes very loud), and the term "explosion" is applied to both processes. "Flammable" applies to a mixture in which any type of combustion can propagate.

Flammability Limits

Hydrogen has a wide range of flammable mixtures with air, being exceeded only by acetylene and hydrazine (ref. 6). The usually recognized upper and lower flammability limits for hydrogen in air saturated with water vapor at ambient temperature and pressure are 74 and 4 percent hydrogen by volume. The 4 percent hydrogen concentration point is called the lower explosion limit (LEL).

Flammability limits are affected by pressure, temperature, and the presence of inert diluents. As the pressure is raised above atmospheric, the range of flammable mixtures narrows up to about 5 atmospheres, then gradually widens as the pressure is raised (ref. 2). As the pressure is lowered, the limits of flammability narrows (refs. 7, 8). Raising the temperature of the gas widens the flammability limits (ref. 7).

The addition of inert gases to hydrogen-air mixtures narrows the flammable range in a manner dependent upon the inert gas. Enrichment by oxygen raises the fuel-rich limit. The rich limit of hydrogen in pure oxygen is about 96 volume percent (ref. 7).

Flame Speed

Flame velocities in hydrogen-air mixtures are given in ref. 2. The maximum velocity is about 300 cm/sec, compared to about 40 cm/sec for methane and propane.

Ignition Energy

The energy required to ignite a mixture near the stoichiometric ratio is quite low, but increases as the flammability limits are approached. The minimum ignition energy required increases as the pressure is lowered (ref. 2). This energy is about one tenth that required to enflame most hydrocarbons. An electrostatic discharge which can hardly be seen or felt can ignite a hydrogen-air mixture (ref. 4). The ease with which hydrogen ignites with air contributes to the burning of accidental leaks of hydrogen. Although no ignition source may be apparent, hydrogen leaks and unflared hydrogen vent stacks often ignite. It is assumed that a small discharge of static electricity is usually responsible, but this has not been conclusively proved (ref. 9). The autoignition temperature is quite high, about 1075°F, compared to 400° to 666°F for most hydrocarbons.

Detonation Limits

The range of detonable mixtures of hydrogen in air is 18 to 59 percent hydrogen by volume. Therefore, not all flammable mixtures are detonable. The occurrence of a detonation wave is dependent upon conditions of confinement, and is especially likely when the mixture is near-stoichiometric, the ignition source is strong, there are confining walls, and the flame path is long. Even partial confinement of hydrogen, for example, by four walls, can be quite violent and destructive, and numerous examples of the damage that can be done are given in the literature (refs. 5, 10, 11). Detonation velocities are shown in ref. 2.

Quenching Distance

When the dimensions of a passage or enclosure containing the gas mixture become small, the heat transfer and/or active particle loss can become great enough to prevent propagation of a flame. When a gas mixture has a certain temperature, pressure, and composition, a resulting flame cannot pass through openings smaller than some minimum size, which is called the quenching distance. This distance depends on the geometry of the passage, but apparently not on the nature of the surface.

This concept is applicable to flame arrestors or flame traps to stop a flame from passing from one place to another. It is of great importance to have adequate flame arrestors in electrical equipment operated around a flammable hydrogen-air mixture. In practice, workable flame arrestors must have openings even smaller than the minimum quenching distance, because there may be a large pressure gradient driving the flame and hot gas toward the arrestor. Fine mesh screens often are used to arrest hydrocarbon-air flames, but the problem is more difficult with hydrogen. Sintered metal, particularly bronze, has been found fairly effective as a flame stopper without greatly impeding the flow of gas (ref. 3). Whether any screen or porous metal practical can fully stop a detonation is in doubt.

Commercially available flame arrestors (Victor, Model 60) were used in these experiments. However, at the delivery pressures anticipated in the "full-up" torch configuration, it is unlikely that these same arrestors will provide adequate protection. The need to provide such arrestors may be a severe limitation on the safety of a high pressure system.

PROPERTIES OF HYDROGEN FIRES

Hydrogen fires and explosions have certain physical properties by which they may be detected. They have fewer observable characteristics than fires involving hydrocarbons.

Flame Temperature

Hydrogen burns in air with a flame that is comparable in temperature to that of most hydrocarbons. For a premixed flame of 43 percent hydrogen in air, the temperature is 3680°F, compared with 3400°F for methane, 3500°F for propane, and 4215°F for acetylene. A diffusion flame, such as that occurring at the site of a hydrogen leak, burns at about 3000°F (ref. 3).

Smoke and Ionization

Pure hydrogen flames burn without smoke. The ionization of hydrogen-air flames is several orders of magnitude lower than that of organic flames, which typically have 10^7 to 10^9 ions cm^3 (ref. 12). Hydrogen flame ionization is so low, in fact, that it is extremely difficult to measure, and can be ruled out, at present, as a detectable flame property.

Optical Radiation

The total electromagnetic radiation emitted from hydrogen-air flames is lower than from many organic flames by a factor of about 10. The total heat radiated by hydrogen fires to personnel and structures is significantly less than is radiated from other, more familiar fires.

For purposes of fire detection, an important consideration is the spectral distribution of the radiation; that is, the amount of radiation emitted in the various wavelength regions of the electromagnetic spectrum. The optical radiation

from pure hydrogen-air flames comes almost entirely from two kinds of molecules, OH and H_2O. These molecules emit ultraviolet and infrared radiation, but neither emits appreciable visible light. Pure hydrogen flames usually can be seen if the surroundings are quite dark; but even with moderate illumination they can be seen only by variations in the transmitted light or "heat wave". Even when the flame location is known, or when it contains some impurities, hydrogen fires often cannot be seen.

Hydrogen Embrittlement

Over a period of years, various NASA facilities have experienced a rash of failures in high-pressure hydrogen storage vessels which were operating well within design limits. In every case the hydrogen was of high purity, typically derived as boil-off from liquid hydrogen, which is at very high purity as a result of the low cryogenic temperatures at which all possible contaminants (with the exception of helium) have been removed as solids. These failures were frequently in the welded sections of vessels that were made up of assembled sections, such as cylindrical sections plus end pieces with fabricated bosses. (This is a significant point because the normal, commercial high-pressure steel "bottle" is typically a one-piece forged unit; so far, these vessels have not experienced the hydrogen environment embrittlement failures).

NASA has indicated that the failed pressure vessels all had similar surface cracking in the vicinity of the ultimate failure. However, the specific mechanism for cracking has apparently not yet been identified. A rough correlation has been achieved, however, between the appearance of the cracked area and the degree of severity with which a given material is attacked. A ranking of "extremely, severely, moderately, etc." is used to denote this degree of severity by the research personnel.

Where a case of "extreme" hydrogen attack is noted, as for certain high-strength Maraging steels, only a few very large cracks are usually noted, with one of these developing into a tensile fracture. On the other hand, "moderately" attacked metals such as the metastable stainless steels of the austenitic family, e.g., SS-304, 305, and 310, show a large number of shallow cracks under hydrogen exposure.

A listing of a number of materials grouped by the degree of severity of the hydrogen environment is presented in Table A4-I. Note that typical low-strength steels are listed as "severely attacked".

A number of conditions have evolved which characterize hydrogen embrittlement failures. Among these are the following:

- Temperatures: Room temperature hydrogen is the most severe case; the problem does not occur at cryogenic temperatures, nor above about 1200°F.
- Pressure: Failures are more severe at high pressure, with one correlation attempting to show a pressure to the one-half power relationship with attack severity.
- Hydrogen Purity: Hydrogen of high purity appears to offer the worst condition for attack. Oxygen as an impurity at 0.6 - 0.7 percent and even lower concentrations has been noted to completely inhibit hydrogen attack by preferential combination with any freshly yielded metal areas. Moisture has a similar effect, but is far less effective than oxygen.

We should note that all of these conditions exist in the contemplated high pressure system. Thus, continuous attention to detail in conjunction with the data contained in Table A4-I will be necessary to ensure safe operation of a high pressure system.

TABLE A4-1

MATERIALS GROUPED BY SUSCEPTIBILITY TO HYDROGEN ENVIRONMENT EMBRITTLEMENT[13]

Extremely Susceptible to Attack	High strength steels
	Maraging
	410, 440C, 430F
	H-11, 4140
	17-4PH, 17-7PH
Severely Attacked	Nickel and nickel alloys
	Nickel 200, 270
	Inconel 625, 70, 718
	Rene 41
	Hastelloy X
	Waspalloy, Udimet 700
	Titanium alloys
	Ti-6Al-4V
	Ti-5Al-2. 5Sn
	Low-strength steels
	Armco Iron, HY-100
	1042, A-302, A-517
	Cobalt alloys
	S-816, HS-188
Moderately Attacked	Metastable stainless steels
	304L, 305, 310
Not Attacked	K-Monel
	Be-Cu Alloy 25
	Pure titanium
	Aluminum and copper alloys
	Stable austeritic stainless steels
	316, 347, A-286

Another condition that appears to be necessary for hydrogen environment embrittlement to occur is that the metal must undergo local or general yielding in the presence of hydrogen. That is, failures have not been experienced in cases of elastic straining of pressure vessels and test specimens. In the case of the pressure vessels that initially failed, causing attention to be given to the problem, it is suspected that local inelastic straining in the areas of discontinuities and weld-associated induced stresses had occurred in the regions of materials failure.

This observation suggests that it may be the welded joints of pipelines where a close examination for susceptibility of hydrogen environment effects should be made in future work.

Cleanliness

Another problem which must be considered is that of cleanliness. All system components in either the hydrogen or oxygen handling side of the system should be vapor degreased prior to installation. In the present series of experiments, elaborate procedures were taken to ensure that the regulators and flow metering valves, in particular, were kept in a clean environment. In the case of oxygen, it is known that disastrous fires have occurred due to the tightening of a threaded joint on an insect. Allowing oxygen to flow across this slightly heated up organic matter was sufficient to encourage combustion. In addition, hydrogen heats up upon expansion at normal temperatures due to the reverse Joule-Thompson effect. Thus, an escaping stream of gas from a high pressure pipe could conceivably reach the ignition temperature and ignite spontaneously. Extreme attention to detail in terms of cleanliness and prevention of castastropic leaks is essential to the safe operation of a system such as described within this report.

DISTRIBUTION LIST

DEPARTMENT OF DEFENSE

Assistant to the Secretary of Defense
Atomic Energy
ATTN: Executive Assistant

Defense Documentation Center
12 cy ATTN: DD

Defense Nuclear Agency
ATTN: DDST
ATTN: TITL
ATTN: SPTD, W. Summa

Field Command
Defense Nuclear Agency
ATTN: FCPR
ATTN: FCTMC, C. Keller

Field Command
Defense Nuclear Agency
Livermore Division
ATTN: FCPRL

Field Command Test Directorate
Test Construction Division
Defense Nuclear Agency
ATTN: FCTC, J. LaComb

Under Secretary of Defense for Rsch. & Engrg.
ATTN: Strategic & Space Systems (OS)

DEPARTMENT OF THE ARMY

Harry Diamond Laboratories
Department of the Army
ATTN: DELHD-N-P

DEPARTMENT OF THE NAVY

Naval Surface Weapons Center
ATTN: Code F31

DEPARTMENT OF THE AIR FORCE

Air Force Weapons Laboratory, AFSC
ATTN: SUL

DEPARTMENT OF ENERGY

Department of Energy
Nevada Operations Office
ATTN: R. Newman

OTHER GOVERNMENT AGENCY

Department of the Interior
U.S. Geological Survey
Special Projects Center
ATTN: R. Carroll

DEPARTMENT OF DEFENSE CONTRACTORS

General Electric Company-TEMPO
ATTN: DASIAC

Pacifica Technology
ATTN: G. Kent

Physics International Company
ATTN: E. Moore

R & D Associates
ATTN: C. MacDonald

SRI International
ATTN: A. Florence

Systems, Science & Software, Inc.
ATTN: R. Duff

Terra Tek, Inc.
ATTN: S. Green

DEPARTMENT OF ENERGY CONTRACTORS

Lawrence Livermore Laboratory
ATTN: Document Control for L-21, D. Oakley
ATTN: Document Control for B. Hudson
ATTN: Document Control for R. Terhune
ATTN: Document Control for J. Shearer

Los Alamos Scientific Laboratory
ATTN: Document Control for R. Brownlee
ATTN: Document Control for E. Jones
ATTN: Document Control for F. App
ATTN: Document Control for A. Davis
ATTN: Document Control for L. Germain

Sandia Laboratories
ATTN: Document Control for C. Mehl
ATTN: Document Control for C. Smith